SEDIMENTOLOGY the journal of the International Association of Sedimentologists

Sedimentology (2019) **66**, 1302–1340 doi: 10.1111/sed.12585

Evolution of a carbonate delta generated by gateway-funnelling of episodic currents

ARNOUD SLOOTMAN*[1], POPPE L. DE BOER†, MATTHIEU J. B. CARTIGNY‡, ELIAS SAMANKASSOU* and ANDREA MOSCARIELLO*
*Department of Earth Sciences, University of Geneva, Rue des Maraîchers 13, Geneva, 1205, Switzerland (E-mail: arnoudslootman@gmail.com)
†Faculty of Geosciences, Utrecht University, P.O. Box 80·115, 3508 TC, Utrecht, The Netherlands
‡Department of Geography, University of Durham, Durham, DH1 3LY, UK

Associate Editor – Gregor Eberli

ABSTRACT

Cool-water carbonate sedimentation has dominated Mediterranean shelves since the Early Pliocene. Skeletal sand and gravel herein consist of remains of heterozoan organisms, which are susceptible to reworking due to weak early cementation in non-tropical waters. This study documents the Lower Pleistocene carbonate wedge of Favignana Island (Italy), which prograded from a 5 km wide passage between two palaeo-islands into a perpendicular, 10 to 15 km wide strait between the palaeo-islands at one side and Sicily at the other during the Emilian highstand (1·6 Ma to 1·1 Ma). The clinoformed carbonate wedge, which is 50 m thick and 6 km long, formed by east/south-east progradation of a platform on the submarine sill by currents that were funnelled between the two palaeo-islands. Platform-slope clinoforms evolved from initial aggradation (thin and low-angle) into a progradation phase (thick and high-angle). Both clinoform types are characterized by a bimodal facies stacking pattern defined by sedimentary structures created by: (i) subaqueous dunes associated with dilute subcritical currents; and (ii) upper-flow-regime bedforms associated with sediment-laden supercritical turbidity currents. Focusing of episodic currents on the platform by funnelling between the islands controlled the downstream formation of a sediment body, here named *carbonate delta*. The carbonate delta interfingers with subaqueous dune deposits formed in the perpendicular strait. This study uses a reconstruction of bedform dynamics to unravel the evolution of this gateway-related carbonate accumulation.

Keywords Antidunes, carbonate delta, chute and pools, cool-water carbonates, cyclic steps, Sicily, subaqueous dunes, supercritical flow, upper-flow-regime bedforms.

INTRODUCTION

Cool-water carbonate production (Lees & Buller, 1972; Schlager, 2000) is controlled by heterozoan organisms (James, 1997), such as bivalves, echinoids, bryozoans, benthic foraminifera and coralline red algae (O'Connell *et al.*, 2016) which live in water depth of tens to

[1] Present address: College of Petroleum Engineering & Geosciences, King Fahd University of Petroleum & Minerals, P.O. Box 5070, Dhahran, 31261, Saudi Arabia

hundreds of metres in the present-day Mediterranean (Fornós & Ahr, 1997). Due to weak early cementation, heterozoan skeletal debris on the sea floor remains unconsolidated (James & Bone, 1989) which, in combination with the absence of reef barriers, facilitates sediment mobilization during storms and occasional currents (Pedley & Carannante, 2006), for example in tidal straits (Anastas *et al.*, 1997; Longhitano, 2013) and marine corridors (Betzler *et al.*, 2006; Puga-Bernabéu *et al.*, 2010).

Physical processes thus govern the redistribution of skeletal sediment on cool-water carbonate sea floors (Fuller *et al.*, 1994; Martín *et al.*, 1996, 2004; Betzler *et al.*, 1997, 2011). Extensive carbonate platforms (in the sense of Read, 1985, and Pomar, 2001) at the storm wave base, fringed with slopes up to a few tens of metres relief (Pomar & Tropeano, 2001), may develop in particular during periods of well-established sea-level stillstands such as the Early Pleistocene (Pedley & Carannante, 2006). A cool-water carbonate platform with a gently sloping surface above storm wave base may be referred to as a distally steepened ramp (Pomar, 2001; Pomar *et al.*, 2002; Massari & Chiocci, 2006). Cool-water carbonate sea floors are scattered with skeletal sand and gravel over potentially the entire length of the depositional profile (Pomar *et al.*, 2002).

The carbonate platform edge does not need to correspond with the shelf edge. Progradation of numerous cool-water carbonate platforms yielded shelf-perched clinoformed prisms (Hansen, 1999; Pedley & Grasso, 2002, 2006; Massari & Chiocci, 2006; Puga-Bernabéu *et al.*, 2010; Massari & D'Alessandro, 2012; Meloni *et al.*, 2013). In terms of physical processes, such carbonate wedges are genetically comparable to the siliciclastic infralittoral prograding wedge of Hernández-Molina *et al.* (2000). An important mechanism for the removal of sediment from cool-water carbonate platforms are currents associated with the offshore migration of subaqueous dunes, which may generate thick sequences of cross-bedded deposits on the platform slope (Pomar & Tropeano, 2001; Pomar *et al.*, 2002; Massari & Chiocci, 2006; Puga-Bernabéu *et al.*, 2008, 2010).

Turbidity current deposits, on the other hand, comprise a substantial part of some cool-water carbonate accumulations (Hansen, 1999; Pomar & Tropeano, 2001; Pomar *et al.*, 2002; Massari & Chiocci, 2006; Puga-Bernabéu *et al.*, 2008). These deposits are commonly attributed to storm events dismantling the sea floor and delivering vast amounts of skeletal debris to the platform edge, where sediment cascades evolve into turbidity currents due to the excess weight of the sediment–water mixture with respect to the ambient seawater. High proportions of shallow water components in such turbidites contrast with the composition of the encasing sediment for which *in situ* production was more important (Pomar, 2001; Pomar *et al.*, 2002; Massari & D'Alessandro, 2012).

Some carbonate accumulations formed in the lee of gateways between the open sea and more restricted basins, by focusing and acceleration of flows through kilometre-wide passages hosting carbonate platforms between palaeo-highs (Lüdmann *et al.*, 2018; Eberli *et al.*, 2019). The depositional nature of such sediment bodies is poorly understood in terms of flow processes. Reconstruction of bedform dynamics from outcrop examples is the key to their understanding.

This study investigates the Pleistocene cool-water carbonate wedge of Favignana Island in southern Italy, interpreted as a platform-slope succession that prograded from a passage between two palaeo-islands, into a larger marine corridor on the Sicily Shelf (Fig. 1). Reconstruction of bedform dynamics on the basis of sedimentary structures reveals that the carbonate sediment body formed by deposition from episodic subcritical and supercritical currents. This type of sediment body is named a *carbonate delta*: a current-controlled carbonate accumulation in the lee of a skeletal-debris-covered submarine sill (cf. Lüdmann *et al.*, 2018).

THEORY: SUBCRITICAL AND SUPERCRITICAL CURRENTS

Flows are either subcritical or supercritical. This is measured by the Froude number:

$$\mathrm{Fr} = \frac{U}{\sqrt{gd}} \quad (1)$$

where U is depth-averaged flow velocity, g is acceleration due to gravity and d is flow thickness. Thus, subcritical flows ($\mathrm{Fr} < 1$) are thick and slow, whereas supercritical flows ($\mathrm{Fr} > 1$) are thin and fast. At the transition of supercritical to subcritical flow, the current goes through a hydraulic jump (Chow, 1959; Long *et al.*, 1991; Lennon & Hill, 2006). Supercritical flows occur in open channels such as rivers (Alexander & Fielding, 1997; Fralick, 1999; Fielding, 2006; Froude *et al.*, 2017) and glacial streams (Duller *et al.*, 2008) and also characterize some submerged flows moving

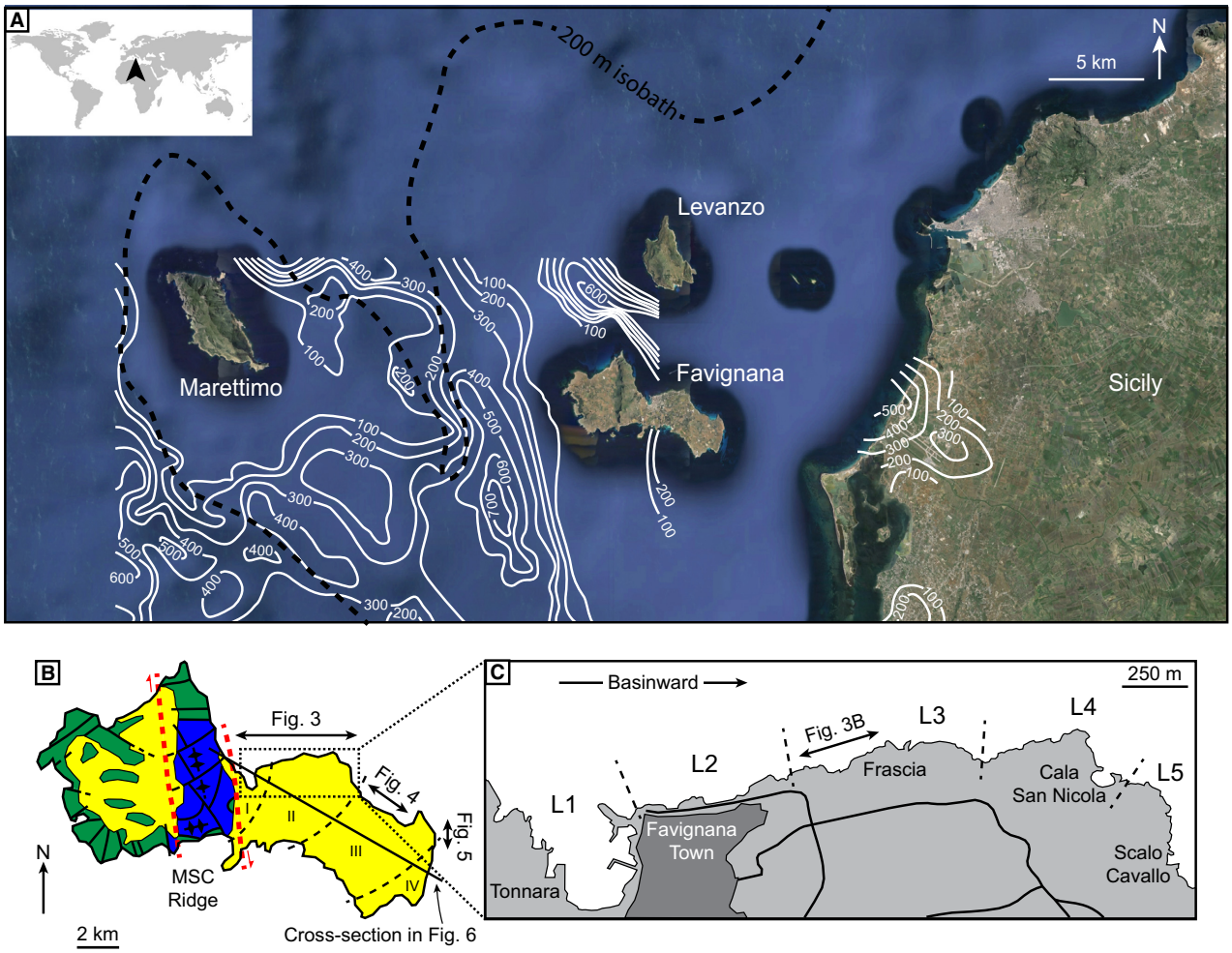

Fig. 1. (A) Location of the study area in the Central Mediterranean Basin. Favignana is the largest island of the Aegadi Archipelago on the western Sicily Shelf. Dashed line indicates present-day shelf edge (200 m isobath). Plio-Quaternary isopachs (ms) from D'Angelo *et al.* (2005) (west) and Catalano *et al.* (2002) (east). Imagery from Google Earth®. (B) Geological map of Favignana (adapted from Abate *et al.*, 1997). Favignana consists of two structural blocks at either side of the deformed Mesozoic–Miocene deposits of the Mount Santa Caterina (MSC) Ridge. The study area comprises the entire eastern part of the island. Roman numerals indicate the spatial distribution of four deposition zones. (C) Close-up of Zones I and II: L1 to L5 correspond to logs in Fig. 3.

over the bed through the water column, such as turbidity currents (Fildani *et al.*, 2006; Turmel *et al.*, 2015; Zhong *et al.*, 2015; Normandeau *et al.*, 2016). For turbidity and other density currents, gravitational acceleration g in Eq. 1 is replaced by submerged gravitational acceleration:

$$g' = g\left(1 - \frac{\rho_{amb}}{\rho_{flow}}\right) \quad (2)$$

where ρ_{amb} and ρ_{flow} are the densities of the ambient water and the flow, respectively. Turbidity currents are intrinsically biased to develop supercritical conditions due to their reduced submerged weight (Postma *et al.*, 2014) on slopes steeper than *ca* 0·5° (Hand, 1974; Sequeiros, 2012; Fricke *et al.*, 2015).

Subcritical and supercritical flows generate lower-flow-regime and upper-flow-regime bedforms, respectively (Carling & Shvidchenko, 2002). The relation between bedform stability and the Froude number has been demonstrated in flume experiments (Yokokawa *et al.*, 2011; Cartigny *et al.*, 2014). These show that subaqueous dunes are out of phase with the upper boundary of subcritical flows and hence migrate downstream by the continued deposition of foreset beds on the bedform lee side (Fig. 2A;

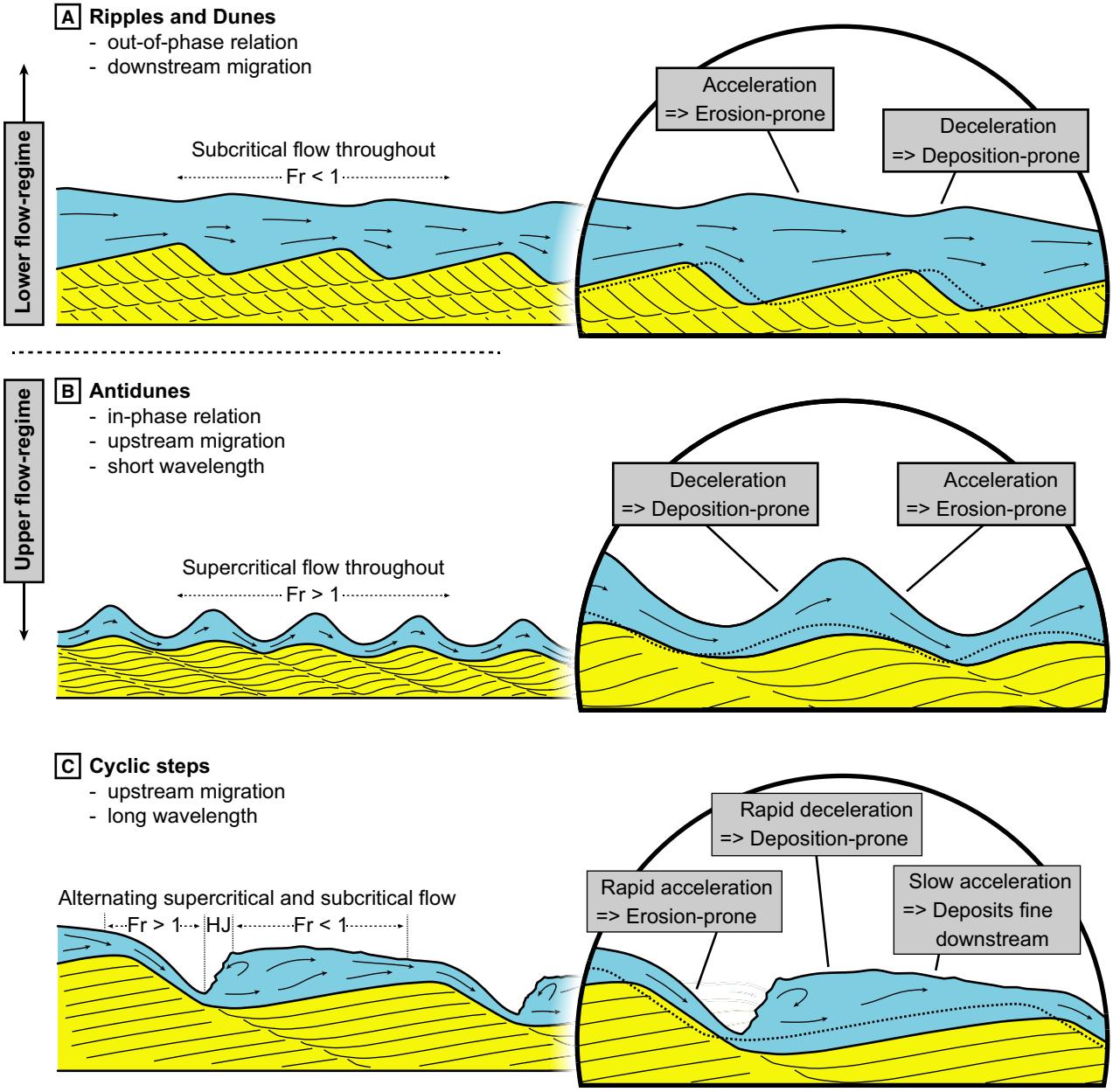

Fig. 2. Bedforms and sedimentary structures of the lower (A) and upper (B) and (C) flow-regimes. (A) Ripples and dunes, forming in Froude-subcritical flow (Fr < 1). (B) Antidunes, forming in Froude-supercritical flow (Fr > 1). (C) Cyclic steps, forming in alternating Froude-subcritical and supercritical flow. HJ: hydraulic jump, which embodies the transition from Froude-supercritical to subcritical flow. Wavelength to flow thickness ratio as shown is representative for antidunes and cyclic steps. Vertically exaggerated for displaying purposes. The sub-aerial-flow dynamics also apply to submerged flows such as turbidity currents.

Kennedy, 1963; Cheel, 1990). With increasing Froude numbers, dunes are washed out and eventually replaced by upper-stage plane bedding (Kennedy, 1963; Saunderson & Lockett, 1983; Cheel, 1990; Carling & Shvidchenko, 2002).

The upper flow-regime, on the other hand, is characterized by supercritical flows with in-phase waves and hydraulic jumps (Kennedy, 1963; Simons *et al.*, 1965; Hand, 1974; Cheel, 1990; Alexander *et al.*, 2001; Spinewine *et al.*, 2009; Yokokawa *et al.*, 2011; Cartigny *et al.*, 2014). Trains of stable antidunes associated with in-phase waves migrate upstream by stoss-side deposition (Fig. 2B; Gilbert, 1914; Kennedy, 1963; Hand, 1974; Cartigny

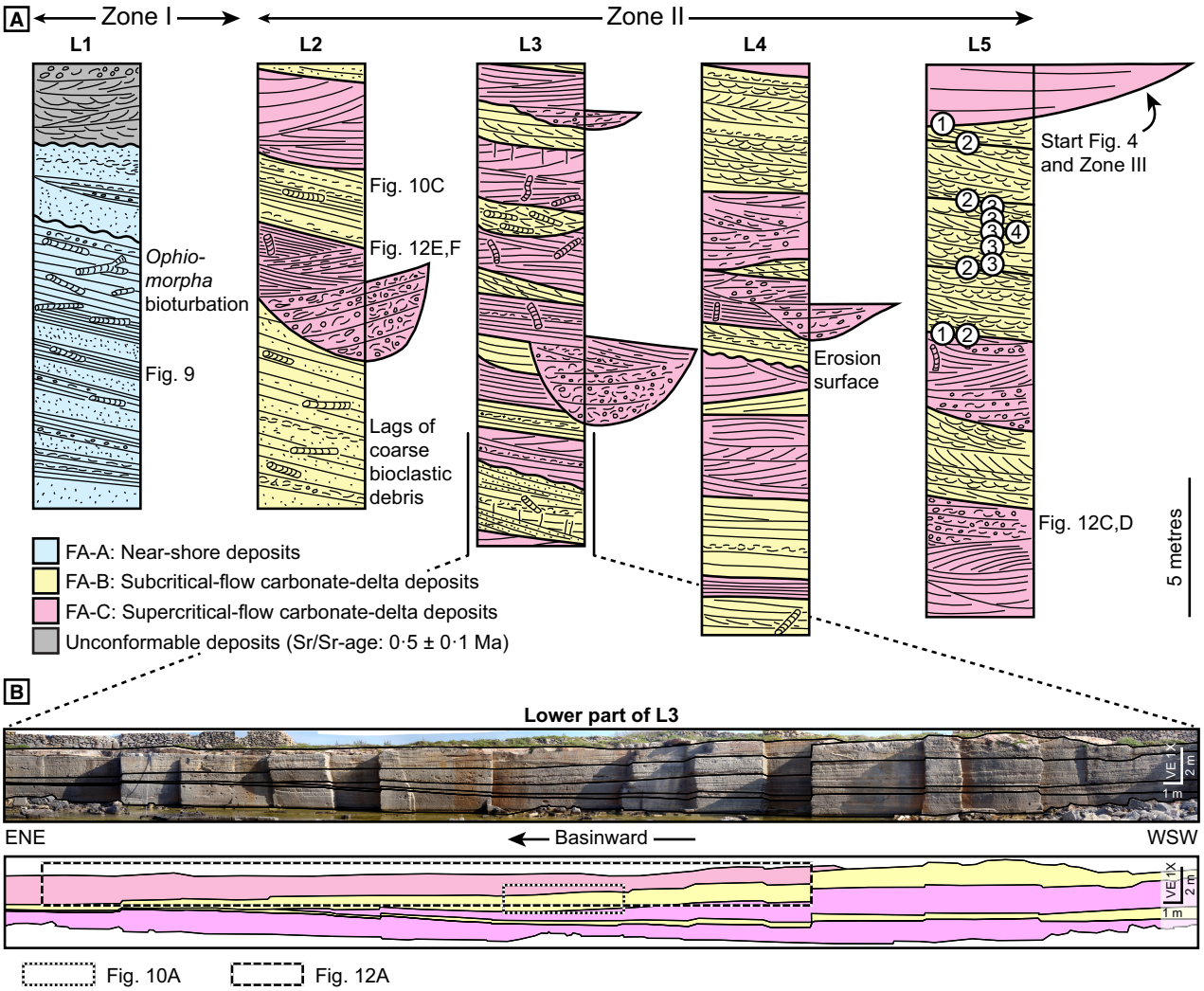

Fig. 3. (A) Schematic composite stratigraphy in Zone I (near-shore environment) and Zone II (platform-top environment) in the north-western part of the study area. Each stratigraphic log (L1 to L5) was measured in coastal outcrops. See Fig. 1 for location. Different colours indicate different facies associations (FA). Note the channel-like appearance of the scour and fill structures of Facies C2 (Fig. 12B to E). Encircled numbers indicate unit boundary hierarchy within FA-B: (1) clinoform unit boundary; (2) set boundary; (3) compound cross-bed boundary; (4) cross-bed boundary. See also Fig. 4. (B) Coastal exposure in Zone II displaying relatively thin and low-angle units that pinch out basinward. Frascia (N37·935411° E12·336681°).

et al., 2014) generating upstream-dipping backset bedding (Davis, 1890; Jopling & Richardson, 1966). With increasing Froude number (Fr = 1·1; Cartigny *et al.*, 2014), stable antidunes are replaced by trains of unstable antidunes in flows marked by growing and breaking in-phase waves (Hand, 1974; Schumm *et al.*, 1982; Alexander *et al.*, 2001; Cartigny *et al.*, 2014). Chute and pool structures (Simons *et al.*, 1965; Hand, 1974; Alexander *et al.*, 2001; Duller *et al.*, 2008; Cartigny *et al.*, 2014) develop where such wave breaking results in a transient hydraulic jump between two antidunes. Ultimately, trains of cyclic steps form (Parker, 1996), typified by supercritical flow down the lee side and subcritical flow over the stoss side of each step, separated by quasi-permanent hydraulic jumps in the troughs (Fig. 2C; Fagherazzi & Sun, 2003; Sun & Parker, 2005; Taki & Parker, 2005; Spinewine *et al.*, 2009; Cartigny *et al.*, 2011; Kostic, 2011; Cartigny *et al.*, 2014; Yokokawa *et al.*, 2016).

GEOLOGICAL SETTING

Favignana is the largest of the three main islands of the Aegadi Archipelago on the

westward continuation of the Sicily Shelf in southern Italy (Fig. 1). Since Late Oligocene times, Sicily has been part of the fold and thrust belt that links the African Maghrebides with Calabria and the Apennines (Catalano *et al.*, 1996; Guarnieri, 2006; Johnston & Mazzoli, 2009), which involved the subduction of initially the Tethys and later the Ionian Ocean plates, and the detachment and deformation of the Mesozoic–Tertiary marine sedimentary cover since the Miocene (Catalano *et al.*, 1996). The southernmost folds and thrusts of the belt continue into the Aegadi Islands (Finetti *et al.*, 1996), where sedimentary Mesozoic units are superposed along the shallow, northward-dipping Favignana Thrust of Early Pliocene age (Incandela, 1995; Tavarnelli *et al.*, 2003). This thrust gave rise to the formation of the north–south-oriented Mount Santa Caterina Ridge, Favignana's principal relief. Post-orogenic extension, controlled by the opening and evolution of the Tyrrhenian Sea (Pepe *et al.*, 2000), generated normal faulting that dissected the Mount Santa Caterina Ridge and overprinted its thrust architecture (Tavarnelli *et al.*, 2003). Two main, dextral strike-slip faults at either side of the ridge separate the island into three structural blocks (Abate *et al.*, 1997). The largest block comprises the entire eastern part of Favignana Island (Fig. 1B). The surface geology of this area (*ca* 10 km^2) is dominated by packstones, grainstones and rudstones, collectively referred to as the 'Favignana Calcarenite' (D'Angelo *et al.*, 2005); they form a wedge up to 50 m thick, which overlies sparsely exposed marlstones of Pliocene age (Monte Narbone Formation of southern Sicily; Slootman *et al.*, 2016a). The carbonate wedge and the Pliocene marlstones are largely unaffected by tectonic deformation and seal most normal and strike-slip faults, although some mild fault reactivation occurred throughout the Quaternary (Tavarnelli *et al.*, 2003).

The age of the Favignana carbonate wedge was constrained using strontium isotope stratigraphy between 1·6 ± 0·1 Ma and 1·1 ± 0·1 Ma, covering a time span of *ca* 500 ± 200 kyr (95% confidence interval) (Slootman *et al.*, 2016a). This age coincides with an important third-order cycle of global sea level recognized in the Pleistocene basins of Sicily (Wornardt & Vail, 1991; Catalano *et al.*, 1998; Pedley & Grasso, 2002). The Favignana carbonate wedge (D'Angelo *et al.*, 2005; Kil & Moscariello, 2012) was interpreted by Ślączka *et al.* (2011) as a bioclastic shoreface system affected by storm-induced and longshore currents and occasional very high-energy events such as tsunamis. The wedge shows a clinoformed architecture (Slootman *et al.*, 2016a) similar to other Plio-Pleistocene carbonate wedges on Sicily (Butler *et al.*, 1997; Catalano *et al.*, 1998; Pedley & Grasso, 2002; Massari & Chiocci, 2006; Massari and D'Alessandro, 2012) and elsewhere in the Mediterranean Basin (Hansen, 1999; Massari *et al.*, 1999; Pomar & Tropeano, 2001; Pomar *et al.*, 2002). On the basis of estimated sediment fluxes, Slootman *et al.* (2016a) proposed that the Favignana wedge formed by the infrequent removal of sediment from a cool-water carbonate platform by subcritical storm-induced currents (average recurrence period: tens to hundreds of years) and supercritical tsunami-induced turbidity currents (average recurrence period: tens of kyr).

METHODS

Favignana offers continuous sea-side and well-exposed quarry outcrops (*Cave di Tufo*) widely distributed across the island. These outcrops were used for the description of lithofacies and clinoform architecture. Stratigraphic sections were measured in the field. Line tracing on photographic panels facilitated defining stratigraphic hierarchies for the reconstruction of bedform dynamics. In addition, close to 100 thin sections were examined. Point counting was performed on 31 thin sections for microfacies analysis (250 counts per sample using JMicroVision v. 1·2·7; see Table S1).

FAVIGNANA CARBONATE WEDGE

Deposition zones, facies associations and composition

The study area is partitioned into four zones (Fig. 1B) on the basis of the distribution of architectural elements and lithofacies. Deposition zones correspond to different positions within the carbonate wedge; proximal (Zones I and II, Fig. 3), medial (Zone III, Fig. 4) and distal (Zone IV, Fig. 5). Four facies associations (FA) were defined on the basis of composition, texture and sedimentary structures (Table 1). Architecture and distribution of facies associations are schematically shown in Fig. 6.

Facies Association A (FA-A) occurs exclusively in Zone I, in the vicinity of the Mount

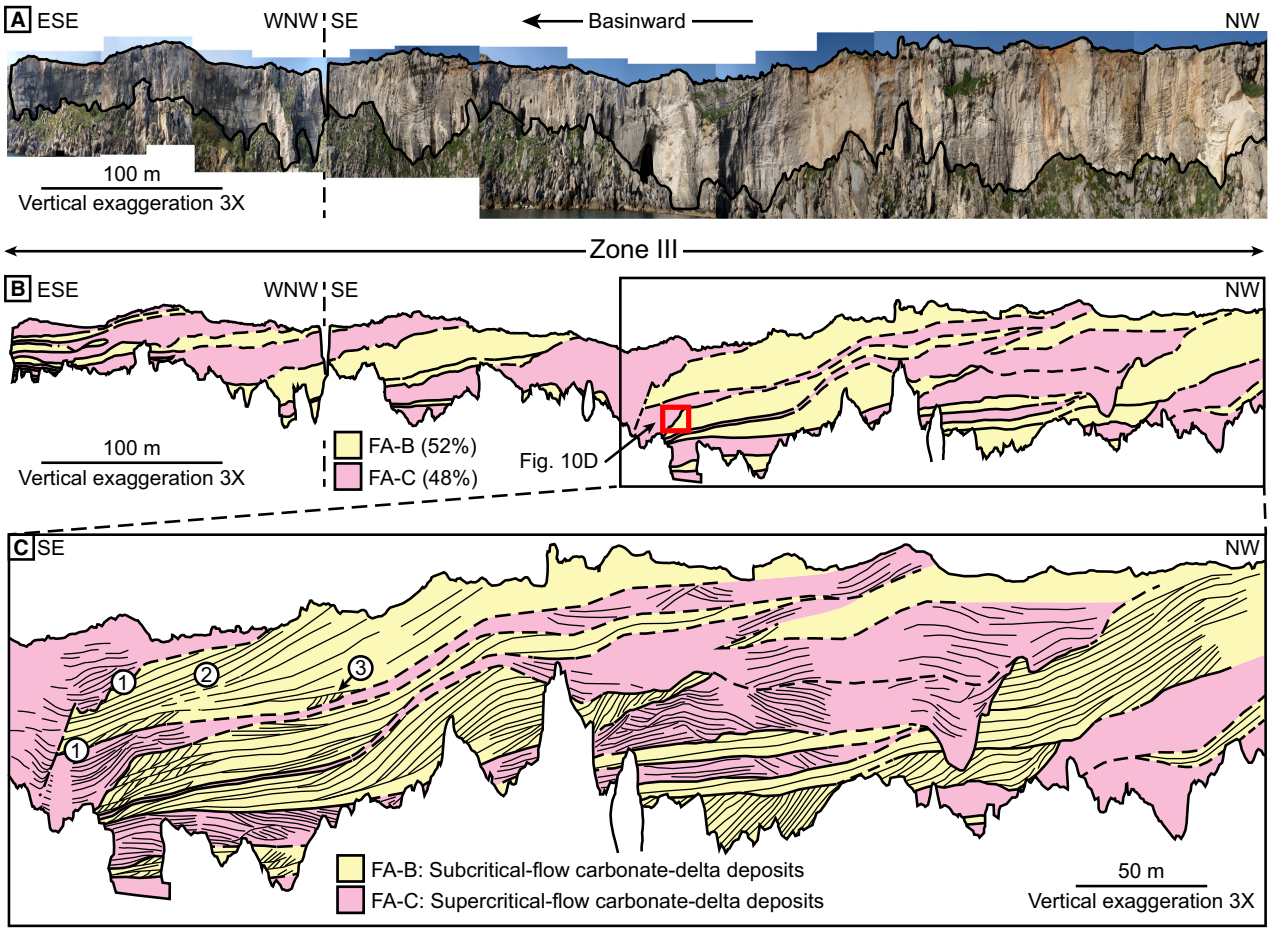

Fig. 4. Clinoform architecture of Zone III (platform-slope environment). See Fig. 1B for location. (A) Vertically exaggerated 'photo-mosaic' of the up to 50 m high Cavallo-Torretta cliff. Recent debris covers the base of the cliff. Note the change in strike in the south-eastern portion of the exposure. (B) Line tracing of internal architecture revealing a bimodal stacking pattern of thick and steep clinoform units resulting from progradation of the platform slope. Facies Association B (FA-B; 52%) was formed by the progradational stacking of subaqueous composite dunes. Facies Association C (FA-C; 48%) was deposited from supercritical turbidity currents (Slootman *et al.*, 2016a). (C) Close-up of north-western part of the cliff displaying the detailed architecture of clinoform units. Encircled numbers indicate unit boundary hierarchy within FA-B: ① clinoform unit boundary; ② set boundary; ③ compound cross-bed boundary.

Santa Caterina Ridge, in the western extremity of the study area. These deposits grade distally into FA-B and FA-C in Zone II, where they occur in a pattern of alternating low-angle units (<5°) up to several metres thick that pinch out basinward. The transition from Zone II to III is marked by a progressive steepening (up to *ca* 20°) and thickening (up to 25 m) of FA-B and FA-C units, developing seismic-scale clinoform units up to 50 m high and 400 to 750 m long, which prograded over a distance of 2 km towards the south-east. The succession of alternating FA-B and FA-C units in Zones II and III comprises by far the largest part of the Favignana carbonate wedge. At the transition from Zone III to IV, FA-B and FA-C clinoform units interfinger with FA-D that predominates Zone IV.

Microfacies analysis reveals that skeletal assemblages are invariably heterozoan (Fig. 7). Unrecognizable fragments make up *ca* 10% on average. With the exception of FA-A, which is dominated by foraminifera, there is little variation in the relative abundance of bivalves, echinoids and foraminifera, together accounting for 40 to 50% of the allochems in FA-B, FA-C and FA-D. The proportion of (carbonate) lithoclasts and serpulids is negligible for all samples.

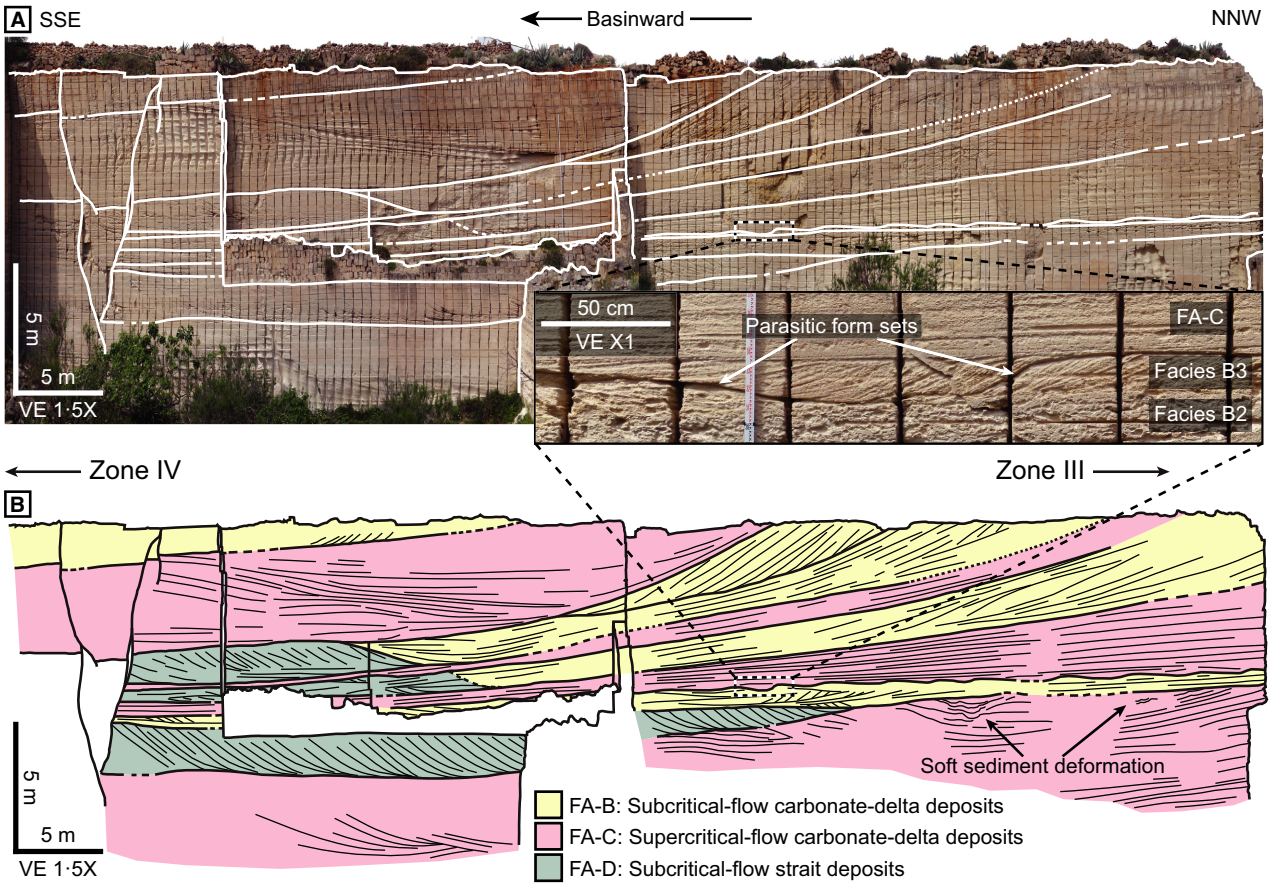

Fig. 5. Architecture of clinoform units at the transition between distal Zone III (toe of slope environment) and Zone IV (strait environment). See Fig. 1B for location. Fra Santo (N37·921132° E12·368542°). Vertical exaggeration 1·5 times. (A) Photograph with the traced boundaries of FA-B, FA-C and FA-D units. Inset shows close-up of parasitic form sets (Facies B3) that are locally present at the top of FA-B units (see also Fig. 10F). (B) Tracing of (A). Note the local soft-sediment deformation structures within the upper part of FA-C units. The strait deposits of FA-D interfinger with the distal, basinward pinching-out clinoform units of FA-B and FA-C.

Differences between samples are largely related to the proportion of bryozoans and coralline red algae. The ratio of bryozoans to red algae is 0·8 (FA-B), 0·4 (FA-C) and 2·2 (FA-D), respectively.

Dip directions of the planar bedding in FA-A, the highest order cross-stratification in FA-B and FA-D, and the master bedding of FA-C are plotted in Fig. 8. These measurements are proposed to indicate palaeoflow directions.

Facies Association A: Near-shore deposits

Description: Facies Association A

Facies Association A formed in the proximity of the Mount Santa Caterina Ridge and grades basinward into FA-B and FA-C. Exposures are restricted to Zone I: FA-A consists of Facies A1 and A2, typically forming pairs, on average 0·5 to 1·0 m thick.

Facies A1: Low-angle parallel-stratified rudstones and grainstones. Grey, irregular-based rudstones and grainstones occur in 20 to 50 cm (rarely >1 m) thick beds that are laterally continuous over tens of metres. Exposures are confined to the foot of the Mount Santa Caterina Ridge (Fig. 9). Facies A1 shows 0·5 to 2·0 cm thick low-angle parallel stratification units with a constant 10° to 15° eastward dip (Fig. 8), some of which display normal grading. Components include fragments of bivalves, coralline red algae, echinoid spines and plates and, in lower abundance, the remains of benthic foraminifera, serpulids, barnacles and rare debris of corals and bryozoans. Coarse basal layers up to 10 cm thick consist of rhodoliths, oyster remains and angular to rounded Mesozoic limestone pebbles and cobbles, some with borings. Bed-parallel to

Table 1. Facies scheme of the Lower Pleistocene carbonate wedge of Favignana Island.

Facies	Texture	Bedding	Primary sedimentary structures	Bioturbation	Composition	Interpretation
Facies Association A: Near-shore deposits						
A1: Low-angle parallel-stratified rudstones and grainstones	Grey rudstones and grainstones	20 to 50 cm thick beds (rarely up to 1 m), later ally continuous over tens of metres	Low-angle parallel stratification (0·5 to 2·0 cm) with 10 to 15° dip towards the east Lags (<10 cm) of rhodoliths and marine-bored oysters and carbonate lithoclasts	Abundant bed-parallel to low-angle inclined *Ophiomorpha nodosa* (Ø < 6 cm, *L* < 1·5 m) with Y-junctions and T-junctions, and few vertical shafts	Fragments of bivalves, coralline red algae, echinoderms. Less common: benthic foraminifera, serpulids, barnacles, coral and bryozoan debris. Contains rhodoliths, marine-bored oysters and carbonate lithoclasts	Continuous wave swash in foreshore environment. Coarse lags are storm-related
A2: Bioturbated packstones and muddy rudstones	Pale yellowish to greenish packstones and muddy rudstones	Few-decimetre thick beds (rarely up to 3 m)	Lenticular, bivalve lags (some articulated). Bioturbation destroyed most pri mary sedimentary structures	*Thalassinoides* abundant. *Ophiomorpha nodosa* less common	As Facies A1, but with a marked abundance in benthic foraminifera. Outsized clasts: bivalves and echinoderms, marine-bored lithoclasts	Sediment baffling in seagrass patches
Facies Association B: Subcritical-flow carbonate-delta deposits						
B1: Bioturbated, cross-bedded rudstones and grainstones/packstones	Bright white to yellowish packstones and muddy rudstones, locally grainstones and rudstones	10 to 30 cm thick cross-beds in 1 to 2 m thick sets (cosets <4 m)	Pervasive *Thalassinoides* bioturbation obliterated any primary structures within cross-beds	*Thalassinoides* abundant, *Ophiomorpha* and *Bichordites* common	Remains of coralline red algae, bivalves, echinoderms, bryozoans and larger benthic foraminifers. Outsized fragments (<15 cm): oysters, *Pecten maximus*, echinoderms and rhodoliths. Minor amounts of lithoclasts. Glauconite is rare	Subaqueous composite dunes formed by the stacking of small parasitic subaqueous dunes. Such bedforms originated in subcritical, unidirectional flows with a dominant S/SE palaeocurrent direction. Lags of large bioclasts suggest incorporation of *in-situ* produced skeletal material
B2: Compound cross-bedded rudstones and grainstones/packstones	Bright white to yellowish rudstones and muddy rudstones, locally grainstones and packstones	10 to 30 cm thick cross-beds, containing subordinate cross-beds of 2 to 10 cm thick (up to angle of repose). Sets: 1 to 4 m thick. Cosets: <6 m in Zone II, <25 m in Zone III	Majority consists of trough cross-bedding. Planar, tangential and sigmoidal cross-bed ding also occur. Lags of outsized skeletal fragments between or within compound cross-beds	*Thalassinoides* common. *Ophiomorpha* rare. Different degrees of bioturbation between and within sets	As Facies B1	As Facies B1

Table 1. (continued)

Facies	Texture	Bedding	Primary sedimentary structures	Bioturbation	Composition	Interpretation
B3: Rudstone and grainstone compound cross-bedded form sets	Bright white to yelowish grainstones and rudstones	Up to 4 m thick compound cross-bedded form sets, displaying original outlines of composite dunes. Compound cross-beds are similar to Facies B2	As Facies B2	*Thalassinoides* common. Different degrees of bioturbation between and within sets	As Facies B1 and B2	As Facies B1 and B2
Facies Association C: Supercritical-flow carbonate-delta deposits						
C1: Wavy-stratified rudstones and grainstones	Bright white to yellowish grainstones and rudstones	Beds 2 to 3 m thick in particular in Zone II, with minor basal erosion. Gradational set boundary is common. Closely associated with Facies C2	Complex interplay of lenses (<30 m wide, <2 m thick) of crudely and spaced-stratified, 2 to 10 cm thick, low-angle, convex to concave cross-stratification	*Ophiomorpha* is present in proximal settings and very rare in distal settings	No outsized macrofossils	Stratification formed by unstable antidunes under breaking in-phase waves
C2: Bio-conglomeratic scour and fill structures	Bright white to yellowish rudstones	Bio-conglomerates fill local, spoon-shaped erosional depressions with depth : length : width *ca* 1 : 2 : 3. Set boundary is composite erosion surface	Internal stratification dips opposite to master bedding, steepness up to 50°	Absence of bioturbation (due to coarseness)	Abundant outsized macrofossils. Basinward decreasing abundance in lithoclasts, oysters and large *Pecten*, increasing abundance in rhodoliths. Local accumulations of echinoids	Chute and pool structures, associated with the strong breaking of in-phase waves due to antidune oversteepening
C3: Backset-stratified rudstones	Bright white to yelowish rudstones	Beds with major basal erosion up to several metres thick. Set boundary is composite erosion surface	Sigmoidal strata (2 to 20 cm thick) dipping opposite to master bedding, in lenticular sets up to 20 m long with shingled stacking pattern, separated by composite erosion surfaces	Absence of bioturbation where coarse-grained. *Ophiomorpha* is very rare where sandier	As Facies C2	Cyclic step bedforms, associated with a series of steps separated by hydraulic jumps in their troughs

Table 1. (continued)

Facies	Texture	Bedding	Primary sedimentary structures	Bioturbation	Composition	Interpretation
C4: Pinching-out planar stratified rudstones	Bright white to yellowish rudstones	Beds <1 m thick. Dominates where FA-C units pinch out distally	Centimetre to millimetre-scale, low-angle cross-stratification, resembling upper-regime plane bedding. Contains local primary current lineation. In places, large-scale undulations	No bioturbation	Composition similar to Facies C1. No outsized clasts	Pinching-out upper-regime plane bedding
Facies Association D: Subcritical-flow strait deposits						
D1: Bryozoan-rich compound cross-bedded rudstones and grainstones/ packstones	Dark yellow to orange rudstones and grainstones	10 to 50 cm thick compound cross-beds (dip typically <20°) in 1 to 3 m thick sets (cosets <15 m). Dip direction of highest order cross-bedding (dip <30°) is highly variable	Majority consists of decimetre-scale trough cross-bedding. Planar and tangential cross-bedding also occur. Lags of outsized skeletal fragments between or within compound cross-beds	*Thalassinoides* common	Bryozoans (>20%), echinoderms, bivalves, larger benthic foraminifera, coralline red algae. Macrofossils: articulated *Pecten*, unbroken echinoids, delicate bryozoans frameworks. Rhodoliths rare	Subaqueous composite dunes formed by stacking of small parasitic subaqueous dunes in the larger strait between the palaeo-islands on one side and Sicily on the other, originating from subcritical, unidirectional flows with a variable palaeocurrent (dominantly north–south). Lags of large bioclasts suggest incorporation of *in situ* produced remains

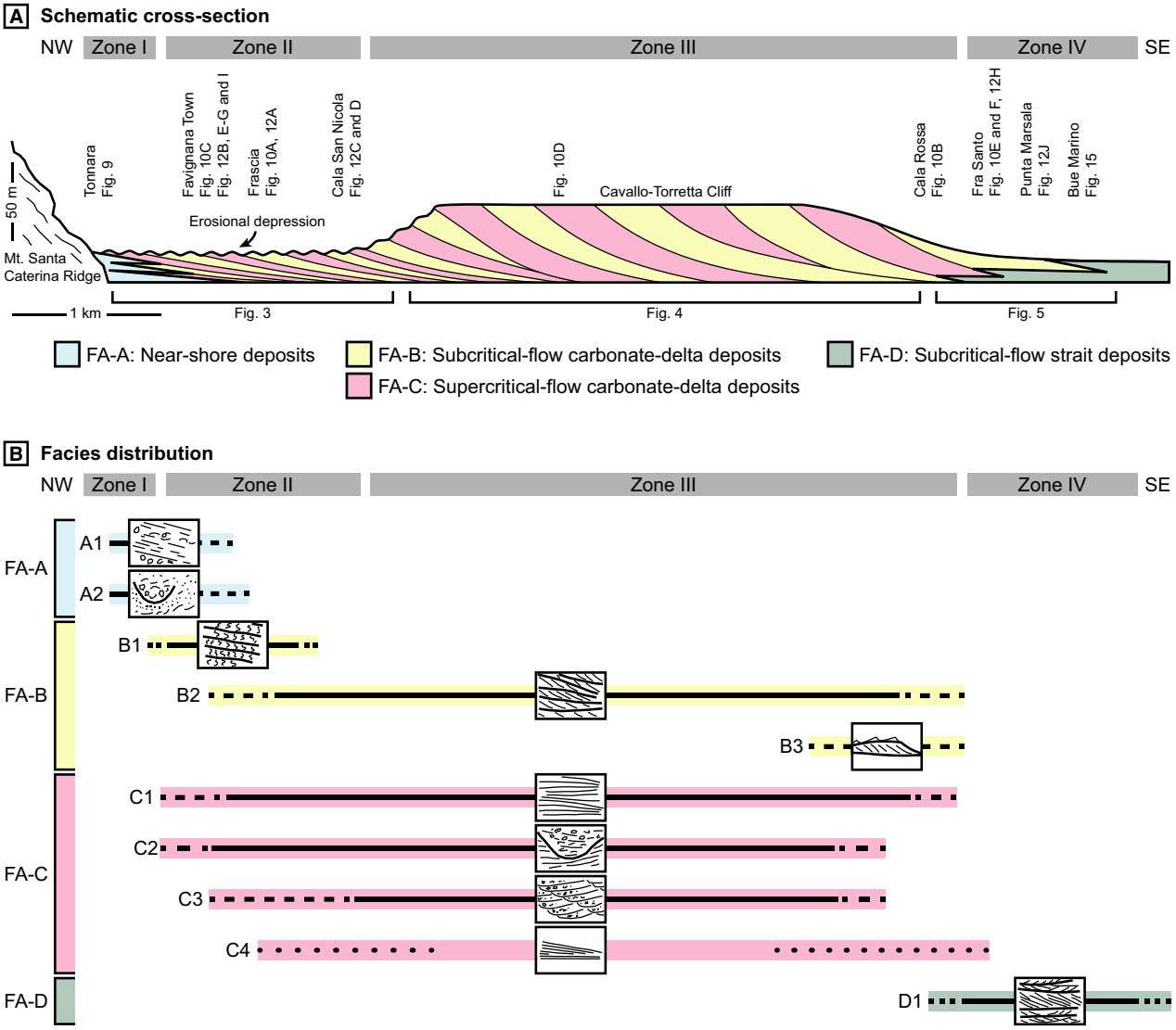

Fig. 6. Deposition zones and facies distributions. (A) Schematic cross-section through the study area. See Fig. 1B for location. Four deposition zones and four facies associations (FA) were identified: FA-A: near-shore deposits, occurring exclusively in Zone I; FA-B: subcritical-flow carbonate-delta deposits; FA-C: supercritical-flow carbonate-delta deposits, occurring in alternation in relatively thin, gently-dipping clinoform units in Zone II and in relatively thick, steeply-dipping clinoform units in Zone III. Clinoform units are locally superposed due to erosion into underlying units or because of the limited distal extent of underlying units; and FA-D: subcritical-flow strait deposits, restricted to Zone IV. (B) The abundance of individual facies is indicated as abundant (continuous), common (dashed) or rare (stippled).

low-angle inclined *Ophiomorpha nodosa* bioturbation up to 6 cm in diameter and 1·5 m in length and with abundant Y-junctions and T-junctions is ubiquitous in some horizons. Vertical shafts connect to more abundant horizontal tunnel networks, penetrating Facies A1 from upper bed boundaries, locally with packstone to wackestone infill. Facies A1 is always encased by Facies A2.

Facies A2: Bioturbated packstones and muddy rudstones. Facies A2 consists of pale yellowish to greenish packstones and muddy rudstones with a composition similar to that of Facies A1, but with a marked abundance of benthic foraminifera (Fig. 7A). Facies A2 alternates with Facies A1 in beds up to several decimetres thick (Fig. 9). Lenticular basal layers with (articulated) bivalve remains occur. Outsized clasts consist

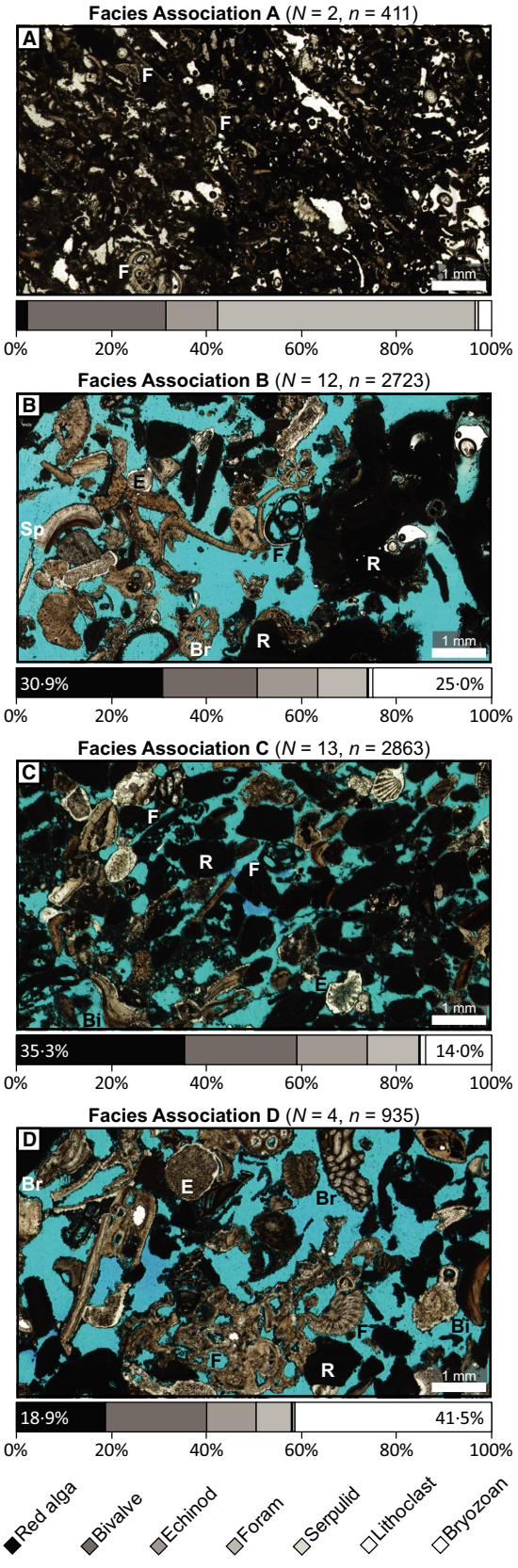

Fig. 7. Thin-section micrographs representing the four facies associations (FA). Space between particles (white and blue shapes) may exceed the true intergranular porosity, as some of the holes were formed during preparation: (A) FA-A (Facies A2), consisting predominantly of foraminifera and relatively fine-grained bioclastic debris. Overall dark impression results from a high proportion of fines. In contrast to the thin sections in (B) to (D), this thin section was not dyed blue; (B) FA-B, coarse-grained rudstone; (C) FA-C, grainstone; (D) FA-D, rudstone. Abbreviations indicate clast composition: Bi = bivalve; Br = bryozoan; E = echinoid; F = foraminifer; R = red alga. *N* = number of analysed thin sections, *n* = number of point counts.

predominantly of bivalve and echinoid fragments and angular lithoclasts with borings. Pervasive *Thalassinoides* and less commonly *Ophiomorpha* bioturbation destroyed primary sedimentary structures in most places and disturbs the contacts with underlying Facies A1.

Interpretation: Facies Association A

Low-angle parallel stratification of Facies A1 is interpreted to have been generated by the swash and backwash of waves on the beach. This is in line with borings in lithic and biogenic components that spent some time in the beach zone as slope debris from the nearby Mount Santa Caterina Ridge. Coarse-grained beds probably reflect the incidence of storms.

Ophiomorpha bioturbation in Facies A1 formed in the depositional environment of Facies A2. During deposition of Facies A2, abundant fine material filled part of vertical *Ophiomorpha* shafts, connected to metre-scale horizontal tunnel networks decimetres below the sediment surface (Gérard & Bromley, 2008). This reflects the absence of mud winnowing in the Facies A2 environment, for example, by the presence of seagrass meadows (Pomar *et al.*, 2002), capable of baffling, trapping and fixing of fines mixed with coarser skeletal components (most notably benthic foraminifera) in a relatively high-wave-energy shallow-water zone (Davies, 1970; Brasier, 1975). Lateral shifting of seagrass meadows could explain the alternation between Facies A1 and A2. Modern *Posidonia* seagrass patches reach up to several metres in height on shallow Mediterranean sea floors down to *ca* 40 m water depth (Fornós, 1988).

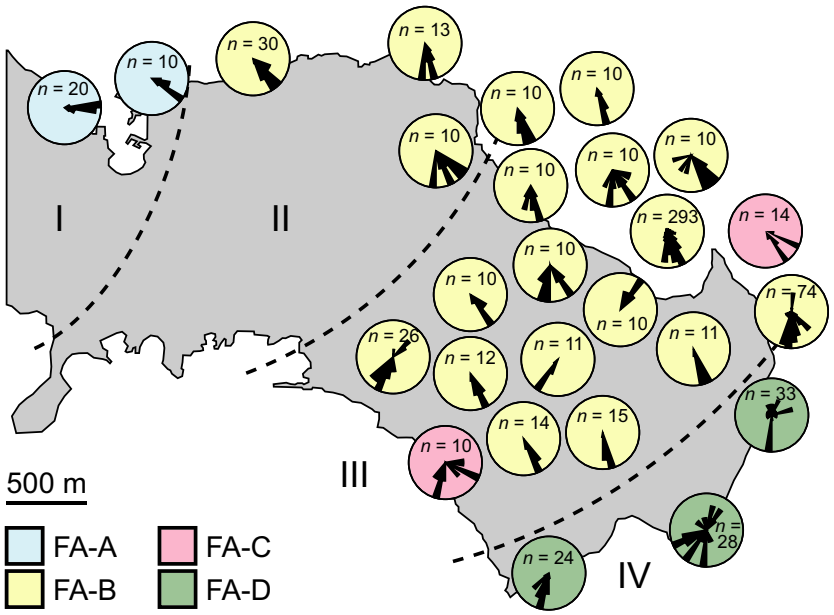

Fig. 8. Spatial distribution of the four deposition zones (roman numerals). Rose diagrams display the dip of the low-angle parallel stratification in FA-A (blue), cross-beds in FA-B (yellow) and FA-D (green) and master bedding in FA-C (pink).

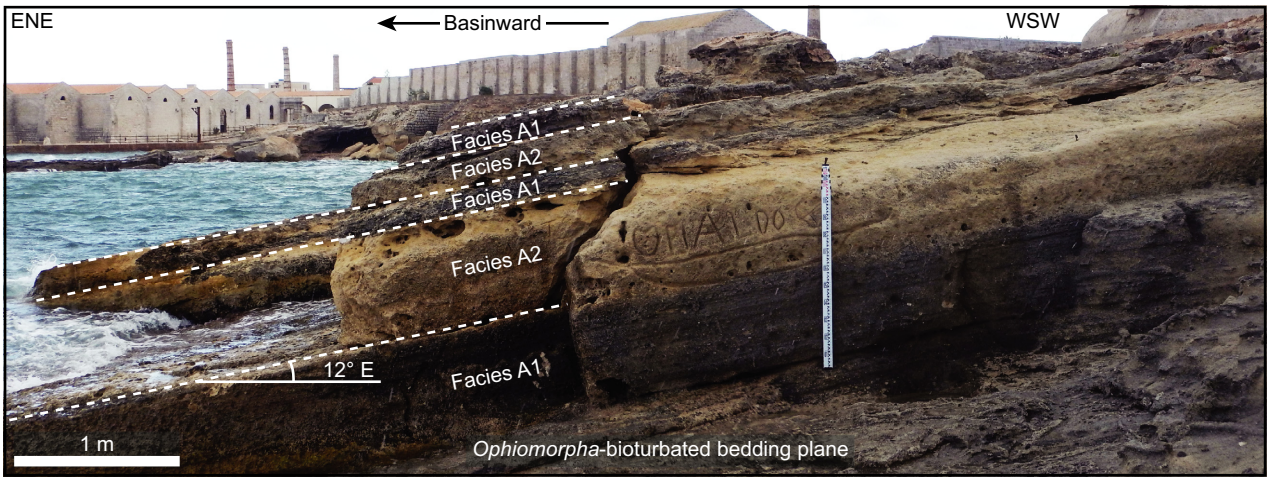

Fig. 9. Facies Association A in proximal Zone I (near-shore environment). Alternation of Facies A1 (foreshore grainstones formed by wave swash) and Facies A2 (packstones formed by sediment trapping in sea-grass patches). Tonnara (N37·932726° E12·321779°).

The reliable identification of fossil seagrass beds is challenging (Brasier, 1975; Reich *et al.*, 2015). Pomar *et al.* (2002) interpreted large-scale cross-stratification ghosts and convex-up structures as the original outline of seagrass patches and moreover refute the possibility that bioturbated packstones represent lagoonal sediment deposited behind grainstone shoals because such settings do not occur in modern Mediterranean environments (references in Pomar *et al.*, 2002). The grading of Facies A2 into the grainy FA-B points to a basinward decrease in abundance of seagrass meadows.

Facies Association B: Subcritical-flow carbonate-delta deposits

Description: Facies Association B

Bright white to yellowish, cross-bedded FA-B deposits constitute approximately half of the Favignana carbonate wedge, the other half consists of FA-C (Fig. 4B). The FA-B units are up to

6 m thick in Zone II (Fig. 3) and up to 25 m in Zone III (Fig. 4): FA-B consistently alternates with FA-C. Towards the distal end of Zone III, where FA-C clinoform units become thinner and eventually pinch out, FA-B units commonly superpose each other, forming seemingly thick, vertically stacked FA-B cross-bedded deposits.

The intensely bioturbated Facies B1 is confined to the proximal sector of Zone II, where it gradually passes landward into the near-shore deposits of FA-A (Fig. 6B). Facies B1 grades basinward into Facies B2, which dominates in Zones II and III. Although consistently present throughout FA-B, the degree of bioturbation decreases basinward. The gently dipping units of Zone II progressively thicken and steepen at the transition with Zone III in which FA-B consists of up to 50 m high clinoform units (Fig. 4). Facies B3 is restricted to the distal part of such clinoform units. The highest order cross-beds dip between south-west and north-east, although predominantly towards the south/south-east (Fig. 8), similar to the progradation direction of the clinoform units in Zone III.

The skeletal sand and gravel of FA-B invariably consist of remains of coralline red algae, bivalves, echinoids, bryozoans and large benthic foraminifera (Fig. 7B). Proportions of these components vary among units and beds, and also within beds. Outsized fossil fragments of oysters, the bivalve *Pecten maximus*, echinoids and rhodoliths up to 15 cm in diameter are locally abundant.

Facies B1: Bioturbated, cross-bedded rudstones and grainstones/packstones. Facies B1 occurs exclusively in the proximal settings of Zones I and II, directly basinward from and interfingering with FA-A around Favignana Town (Fig. 6). It has a variable mud content that generally decreases basinward, where packstones and muddy rudstones grade into grainstones and rudstones. Facies B1 consists of 10 to 30 cm thick cross-beds (③ in Fig. 10A) bundled in sets about 1 to 2 m thick (② in Fig. 10A) that pinch out laterally and basinward (Fig. 3B). Vertically stacked sets (cosets) are rarely thicker than 4 m. Sets dip gently (*ca* 5°) towards the east/south-east. Cross-bedding is commonly only slightly steeper (5° to 10°, up to 20°) and downlaps gently onto lower set boundaries. Pervasive *Thalassinoides* and less abundant *Ophiomorpha* bioturbation obliterated primary sedimentary structures within and, in places, between cross-beds. Compound cross-bedding of Facies B2 occurs locally within Facies B1 sets (Fig. 10A), progressively replacing Facies B1 basinward.

Facies B2: Compound cross-bedded rudstones and grainstones/packstones. Facies B2 predominates in Zones II and III, forming 1 to 4 m thick, compound cross-bedded sets (② in Fig. 10B and D). Compound cross-beds (③ in Fig. 10) are 10 to 30 cm thick and consist internally of higher-order cross-beds 2 to 10 cm thick (④ in Fig. 10). Finer material generally constitutes thinner cross-beds, whereas coarser sediment comprises the thicker ones. Such higher-order cross-beds dip up to *ca* 30°. Compound cross-beds in which such higher-order cross-beds occur, have lower dips (up to 25°) and downlap at slight angles onto lower set boundaries. Most set bases are regular erosion surfaces. Some Facies B2 deposits in distal settings are confined to depressions at the top of FA-C.

Most Facies B2 sets (② in Fig. 10B and D) dip towards the south-east. The dip direction of compound cross-bedding (③ in Fig. 10) consistently follows the dip of the containing sets. The dip of the highest-order cross-beds (④ in Fig. 10) is more variable. Usually, such subordinate cross-beds dip in the same direction as sets and compound cross-beds; but may be more variable where the latter have very gentle inclinations (from near-horizontal up to 7°), particularly in the toe sets of FA-B clinoform units in Zone III.

Reactivation surfaces separating compound cross-beds are common (Fig. 10D). The upper part of compound cross-beds (③ in Fig. 10) is typically truncated by overlying set boundaries (② in Fig. 10B and D). In places, where such cut-off is minimal, sigmoidal geometries are preserved (Fig. 10D). The majority of compound cross-beds consist internally of trough cross-bedding (④ in Fig. 10). Also compound cross-beds themselves (③ in Fig. 10) locally occur in sets (② in Fig. 10B and D) marked with trough architectures 10 to 20 m wide, for example in the eastern cliffs of Cala Rossa (Fig. 10B).

Distal and vertical stacking of Facies B2 sets are common, forming cosets (① in Fig. 3) up to 6 m thick in Zone II. Such cosets significantly thicken basinward and reach up to 25 m in the proximal part of progradational clinoform units in Zone III (Fig. 4). Here, significant variations in set thickness occur and compound cross-beds attain steeper dips associated with steeper lower set boundaries. Basinward in Zone III, cosets of Facies B2 occasionally superpose one another

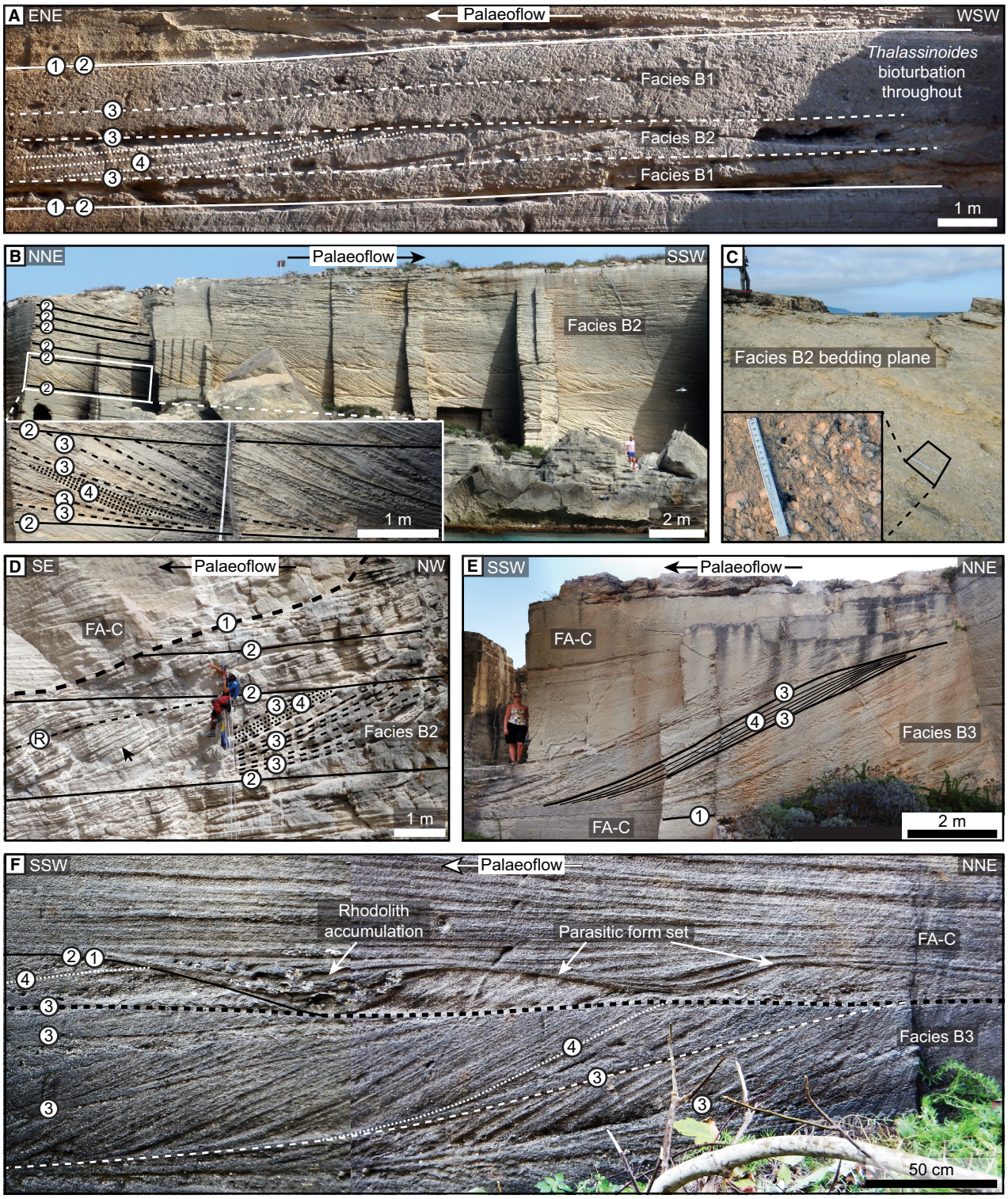

where FA-C units no longer separate them because they have pinched out (for example, the Cala Rossa locality; Fig. 10B). This causes vertical stacking of Facies B2 sets into anomalously thick packages in some clinoform unit toe sets. Eventually, Facies B2 units thin and pinch out basinward at the transition with Zone IV (Fig. 5).

The majority of Facies B2 is composed of coarse skeletal material that forms rudstones, along with grainstones and packstones. No

Fig. 10. Exposures of Facies Association B. See Fig. 6A for locations. Encircled numbers indicate unit boundary hierarchy within FA-B: ① clinoform unit boundary; ② set boundary; ③ compound cross-bed boundary; ④ cross-bed boundary. (A) Close-up of coastal outcrop in Fig. 3B revealing a set of Facies B1 cross-bedding and Facies B2 compound cross-bedding in Zone II. Both facies are formed by the migration and progradation of subaqueous composite dunes but are affected by different degrees of bioturbation. Frascia (N37·935411° E12·336681°). (B) Thick FA-B units that were vertically stacked due to the pinching-out of FA-C units proximal to this location. Cala Rossa (N37·922869° E12·365926°). (C) In places, coarse lags of bioclastic debris occur between compound cross-beds. Ruler – centimetre scale. Punta San Leonardo (N37·934758° E12·332913°). (D) Close-up of Cavallo-Torretta Cliff in Fig. 4B (Zone II) showing variation in the dip-angle and thickness of compound cross-beds and sets. Dip direction is unimodal. Note the sigmoidal geometries (arrow) and reactivation surfaces (®). (N37·927532° E12·352753°). (E) Compound cross-bedded form sets of Facies B3 in distal Zone III (toe of slope environment), preserving the outlines of large subaqueous composite dunes. Fra Santo (N37·923437° E12·367268°). (F) Parasitic form sets of Facies B3 on the upper boundary of a compound cross-bedded form set. These structures were created by parasitic dunes that migrated over the stoss side of a parent composite dune prior to rapid burial by FA-C. Fra Santo (N37·922787° E12·367429°).

proximal to distal trend in grain-size distribution was observed. Marine fossils, most notably up to 15 cm large bivalves, echinoids and fragments of red algae, are locally abundant in lags (Fig. 10C), occurring between or dispersed within compound cross-beds. Many of such body fossils include intact echinoid shells and articulated bivalves. *Thalassinoides* bioturbation is common in all Facies B2 exposures, the degree of which varies between and within sets. Some bedding planes show abundant *Bichordites* bioturbation. In the proximal part of Zone II, where Facies B2 occurs as a minority in sets predominantly composed of Facies B1 (Fig. 10A), the degree of *Thalassinoides* bioturbation is commonly much higher than in more basinward locations.

Facies B3: Rudstone and grainstone compound cross-bedded form sets. Facies B3 is restricted to the outer limits of Zone III where clinoform units thin and eventually pinch out. Rudstones are predominant and occur in up to 4 m thick, compound cross-bedded form sets (*sensu* Imbrie & Buchanan, 1965) (Fig. 10E and F). They are similar to Facies B2, with the difference that Facies B3 units have preserved the outlines of large (*sensu* Ashley, 1990) subaqueous composite dunes. Form sets are variably underlain by FA-B or FA-C, but are consistently overlain by FA-C (Fig. 10E and F). The preserved stoss side (upstream face) of composite dunes are up to tens of metres long, whereas lee sides do not exceed 10 m in length. Because stoss sides display low angles (up to 5°) with the bases of form sets (which themselves also have low-angle dips), preserved stoss sides are near-horizontal in outcrop (Fig. 10F). Form sets are typically covered by 'parasitic' form sets, formed by relict, small (*sensu* Ashley, 1990; 1 to 3 m spacing) subaqueous dune fields covering near-horizontal surfaces of hundreds of square metres (Fig. 10F). The cross-beds (④ in Fig. 10F) in small parasitic form sets commonly dip in the same direction as compound cross-beds (③ in Fig. 10F) and subordinate cross-bedding within them (④ in Fig. 10F). Parasitic dune fields also rarely occur on Facies B2, where upper set-boundaries are near-horizontal and overlain by FA-C (inset in Fig. 5A).

Interpretation: Facies Association B

Facies Association B occurs in Zones II and III in an extensive part of the study area. The appearance of the different FA-B facies varies as a function of the degree of bioturbation and progradational character. Pervasively bioturbated Facies B1, occurring exclusively in the most proximal settings, grades basinward into the less intensely bioturbated Facies B2. In Zone II, both Facies B1 and B2 comprise sets (② in Fig. 11) with cross-stratification (③ in Fig. 11) comparable in size. However, only in Facies B2 the lower degree of bioturbation enables the recognition of a higher-order cross-bedding (④ in Fig. 11). The occurrence of Facies B2 compound cross-beds within sets of Facies B1, suggests that these facies are genetically related, having a similar formative process, and that the pervasive bioturbation of Facies B1 later obliterated the highest-order cross-bedding. This can be the result of lower rates of sediment supply (i.e. the sum of transported and *in situ* produced material) in the proximal portion of Zone II relative to Zone III under comparable intensity of biotic activity (Martín *et al.*, 1996; Pomar, 2001; Pomar *et al.*, 2012).

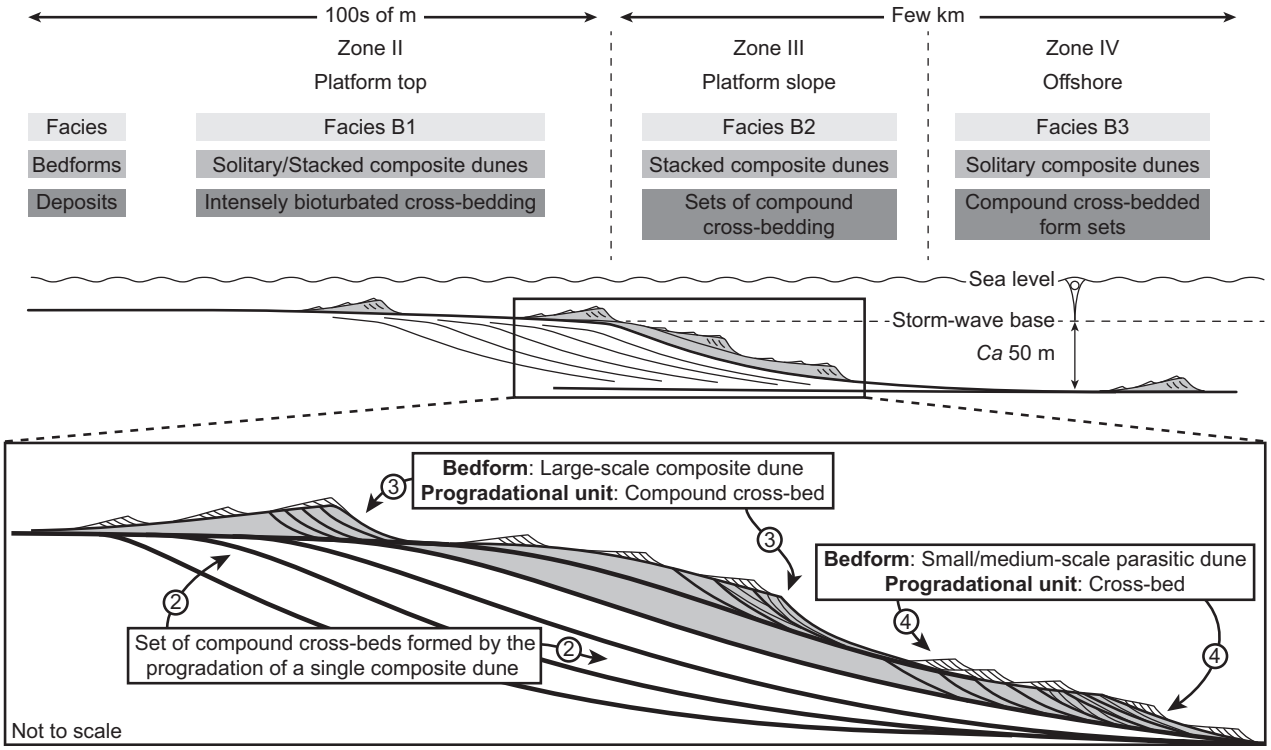

Fig. 11. Interpretation of Facies Association B within each zone and inferred depositional environment, together with the interpretation of bedforms and the nature of the resulting deposits. Internal organization of unit-boundary hierarchy is explained in the inset (see also encircled numbers in Fig. 10). Modified after Slootman *et al.* (2016a).

The proximal parts of FA-B clinoform units (① in Fig. 4C) in Zone III are composed of steep and thick Facies B2 sets (② in Fig. 11), emphasising a strongly progradational character. Basinward, towards clinoform unit toe sets where Facies B2 sets thin and eventually pinch out, form sets of Facies B3 occur. Form sets are created by the burial of cross-stratified bedforms preserving their original outlines (Imbrie & Buchanan, 1965; see review by Allen, 1982, and Anastas *et al.*, 1997). The formative bedforms of Facies B3 encompass large (Ashley, 1990; 10 to 100 m spacing, 0·75 to 5·0 m height) and medium (Ashley, 1990; 5 to 10 m spacing, 0·4 to 0·75 m height) subaqueous composite dunes, formed by the stacking of subordinate, small (Ashley, 1990; 0·6 to 5·0 m spacing, 0·075 to 0·4 m height) subaqueous dunes. Such parasitic bedforms migrated up the stoss side of the larger parent bedforms. Upon reaching the crest, these commonly three-dimensional parasitic dunes migrated down the lee side of the composite dune, where they formed trough cross-stratified beds of decimetre-scale thickness (④ within ③ in Figs 10 and 11), which are referred to as compound cross-beds (Allen, 1982, and references therein; see also Anastas *et al.*, 1997).

Composite dunes climb up one another's stoss side under conditions of sufficient sediment supply, such as in the depositional environment of Facies B2. In particular where sufficient accommodation space was available, such as in the slope environment of Zone III, compound cross-bedded sets stacked into thick cosets (Fig. 11). In environments with low rates of sediment supply, such as clinoform toe sets, the sea floor was covered by migrating composite dunes that were unable to climb and therefore remained solitary (Slootman *et al.*, 2016b). Such composite dunes and their subordinate parasitic dunes were preserved in the sedimentary record when rapidly blanketed by FA-C during high-energy events. A near-horizontal discordant surface (black dashed line in Fig. 10F) marks the contact between the compound cross-beds of the parent dune (below) and the decimetre-scale parasitic dunes (on top) that 'shaved' the stoss side of the parent dune. The preservation of small dunes (parasitic form sets) resulted in the preservation of widespread, relict dune fields (inset in Fig. 5A).

The variability in the thickness and degree of bioturbation of compound cross-beds demonstrates that Facies B2 and B3 were formed by the stacking of decimetre-scale dunes that migrated during numerous episodes of flow activity. Such episodes were separated by significant periods of exposure at the sea floor, evidenced by densely bioturbated surfaces, reactivation surfaces and coarse bioclastic lags within Facies B2 and B3. The macrofossils forming lags (Fig. 10C) are the remains of organisms that lived *in situ* on the sea floor during breaks in sedimentation. Under renewed flow activity such coarse material was transported and preserved as lags covering entire lee sides or incorporated into compound cross-beds rich in large fragments of bivalves, echinoids and coralline red algae.

The dip direction of the highest-order cross-bedding (④ in Fig. 10) reveals the migration direction of the smallest dunes. The limited distribution of Facies B2 in proximal settings prevented the detailed estimation of palaeoflow in Zone II. In contrast, the numerous dip directions of cross-bedding measured in Zone III suggest that palaeoflow was dominantly towards the south-east, with a subordinate direction towards the south-west (Fig. 8). In distal exposures, the dip of high-order cross-beds suggests an additional northward palaeoflow. Such high-order cross-beds (④ in Fig. 10), however, occur in southward-dipping compound cross-beds (③ in Fig. 10). These anomalous structures form a minority and are restricted to very gently inclined sets (from near-horizontal up to 7°). This suggests that the smallest bedforms locally also migrated up the lee side of parent bedforms, although were not capable of altering the migration direction of large composite dunes. Where the sea floor was too steep, such as in the proximal part of Zone III, bedforms were incapable of migrating upslope. Hence, the majority of cross-beds in the slope settings of Zone III resulted from slope-perpendicular currents, although along-slope currents might have played a minor role here. However, a slight deflection of slope-perpendicular currents towards the right (see also Hernández-Molina *et al.*, 2000; Massari and D'Alessandro, 2012) might be a result of the Coriolis force (Puga-Bernabéu *et al.*, 2010), explaining the minor proximal–distal clockwise rotation in the dip direction of FA-B (and FA-D) cross-beds (Fig. 8). However, more slope-parallel currents affecting the sea floor beyond toe of slope settings (Longhitano & Steel, 2016; Michaud & Dalrymple, 2016; Rossi *et al.*, 2017) cannot be excluded either.

Facies Association C: Supercritical-flow carbonate-delta deposits

Description: Facies Association C

Facies Association C comprises thick units that have been deposited as single beds. They are bright white to yellowish and reach up to 4 m thickness in Zone II and over 10 m in Zone III, where deep basal scours are common (Fig. 4). The toe sets of FA-C clinoforms pinch out over short distances (for example, from 4 to 0 m thick over a down-dip length of *ca* 100 m; Fig. 5). Facies Association C is composed largely of rudstones and rare grainstones; packstones are absent: FA-C encompasses approximately half of the Favignana carbonate wedge; the other half is formed by FA-B. Homogeneous FA-C deposits were the target of widespread quarrying activities across the island, providing the exceptional exposures.

Facies Association C consists of four facies in Zones II and III (Fig. 6). The wavy-stratified Facies C1 and the associated bio-conglomeratic scour and fill structures of Facies C2 are most abundant in Zone II. Facies C3 is dominated by backset-bedding and prevails in Zone III. At the distal termination of FA-C clinoforms, where beds eventually pinch out, the planar stratified Facies C4 occasionally occurs (Table 1).

The composition of FA-C is similar to that of FA-B (Fig. 7), although with lower proportions of bryozoans in favour of red algae. In Zone II, the largest components consist mainly of bivalve debris, dominated by *Pecten maximus* and fragmented oysters. Rhodoliths make up large portions of the bio-gravel in Zone II and become nearly exclusive for the coarse fraction in Zone III. Lithoclasts of various composition rarely reach 10% in abundance.

The near absence of *Thalassinoides* and the very rare occurrence of *Ophiomorpha* in FA-C stand in sharp contrast to the locally pervasive bioturbation of FA-B. The very rare *Ophiomorpha* is limited to Zone II, occurring in small networks of horizontal tunnels and vertical shafts, which reach down to 1·5 m below upper bed boundaries. Some long vertical shafts (up to 4 m) are not connected to horizontal tunnels.

Facies C1: Wavy-stratified rudstones and grainstones. Facies C1 consists of rudstone and grainstone beds of 2 to 3 m thick, making up the

majority of FA-C in Zone II. Internal stratification is expressed by the virtue of minor grain-size variations, ranging from coarse sand to coarse granule-size skeletal fragments. In most places such stratification consists of alternating coarsening and fining-upward intervals of 2 to 10 cm thick (diffuse banding, e.g. Postma *et al.*, 1983; or crude stratification, e.g. Cartigny *et al.*, 2013; Postma *et al.*, 2014). Locally, stratification consists of coarsening-upward layers with sharp, erosional bases (spaced stratification of Hiscott, 1994).

The wavy stratification forms lenticular sets, with concave bases and convex tops, which are up to *ca* 20 m wide and 1 to 2 m thick, that are best exposed in long, sea-side quarry walls (Fig. 12A). Where composed of Facies C1, FA-C units usually display straight, erosional upper boundaries inclined more or less parallel to the inclined lower boundaries. The latter are rarely erosional, draping the uneven topography of the underlying FA-B (Fig. 12A). Internal stratification is thicker and coarser in the central portion of sets compared to the thinner and finer-laminated extremities. Lamination does not terminate at set boundaries, but becomes very thin and continues into adjoining sets, herewith creating apparent downlaps on these vaguely defined surfaces (Fig. 12A and B). *Thalassinoides* bioturbation is absent from the main body of units, but locally affected the uppermost part of Facies C1 beds (Fig. 12B). *Ophiomorpha* structures form vertical shafts, which are commonly connected to horizontal tunnels that become rare basinward. The interwoven stratification of Facies C1 is often truncated by the bio-conglomeratic scour and fill structures of Facies C2 (Fig. 12B).

Facies C2: Bio-conglomeratic scour and fill structures. The matrix-supported to clast-supported biogenic conglomerates of Facies C2 encompass the coarsest sediments of the Favignana carbonate wedge. They are most abundant in Zone II and occur in close association with Facies C1 (Fig. 12B). Large clasts are up to 15 cm in diameter and composed of rhodoliths, oysters, *Pecten maximus* and lithic fragments. Rhodoliths gradually replace the other outsized components in basinward direction. The coarse deposits of Facies C2 lack bioturbation.

The bio-conglomerates fill erosional depressions about 1 to 4 m deep, with depth : width : length ratios approximately 1 : 2 : 3 (Fig. 12C to F). Scour and fill structures are locally fining upward and typically have spoon-shaped geometries with the long axis striking approximately south/south-east and the gentle side facing basinward. Scour and fill structures are vertically or laterally stacked (Fig. 12B and G) and also occur as isolated bodies (Fig. 12C to F).

The scour and fill structures of Facies C2 commonly cut into Facies C1 and more rarely into FA-B. Very irregular set boundaries at lateral and proximal sides are inclined up to 70° (Fig. 12F). Very coarse fills have a massive appearance complicating the identification of internal stratification. However, steep cross-beds up to 20 cm thick and often exceeding the angle of repose (up

Fig. 12. Exposures of Facies Association C. See Fig. 6A for locations. (A) Close-up of coastal outcrop in Fig. 3B consisting of wavy stratification of Facies C1, generated by unstable antidunes under breaking in-phase waves. Dashed lines indicate set boundaries. Note 2·5 times vertical exaggeration. Frascia (N37·935411° E12·336681°). (B) Wavy stratification of Facies C1 and scour and fill structures of Facies C2 in Zone II, interpreted as unstable antidune stratification and chute and pool structures, respectively. Landro (N37·927676° E12·329619°). (C) to (F) Scour and fill structures of Facies C2 in Zone II interpreted as confined chute and pool structures. Note that the backset-bedding in (C) and the lower unit-boundary in (F) are much steeper than the angle of repose, providing additional evidence against a channel-fill hypothesis. Asterisks in (E) and (F) indicate the same location for comparison. (C) and (D) Cala San Nicola (N37·934601° E12·347574°). (E) and (F) Punta San Leonardo (N37·927676° E12·329619°). (G) Two stacked Facies C2 scour and fill structures. Palaeoflow left oblique towards the observer. Cava Sant'Anna (N37·931421° E12·331066°). (H) and (I) Facies C3 backset-stratification interpreted to have been generated by cyclic step bedforms. Diagnostic criteria include upstream-dipping stratification and set boundaries that are composite erosion-surfaces (CES). Close-up of CES in (H), juxtaposing relatively coarse and fine sediment. Fra Santo (N37·922524° E12·368346°). The exposure in (I) shows three progradationally stacked Facies C3 sets. Backset beds are fining downstream. They are concave-upward in their upstream portion and tend to become convex-upward towards their downstream end. The middle set is very coarse, consisting predominantly of large bivalves (*Pecten maximus*) and oysters. Badia (N37·929329° E12·332747°). (J) Facies C4 planar stratification interpreted as upper-stage plane bedding, occurring at the basinward termination of some FA-C clinoform units. Punta Marsala (N37·907261° E12·364657°).

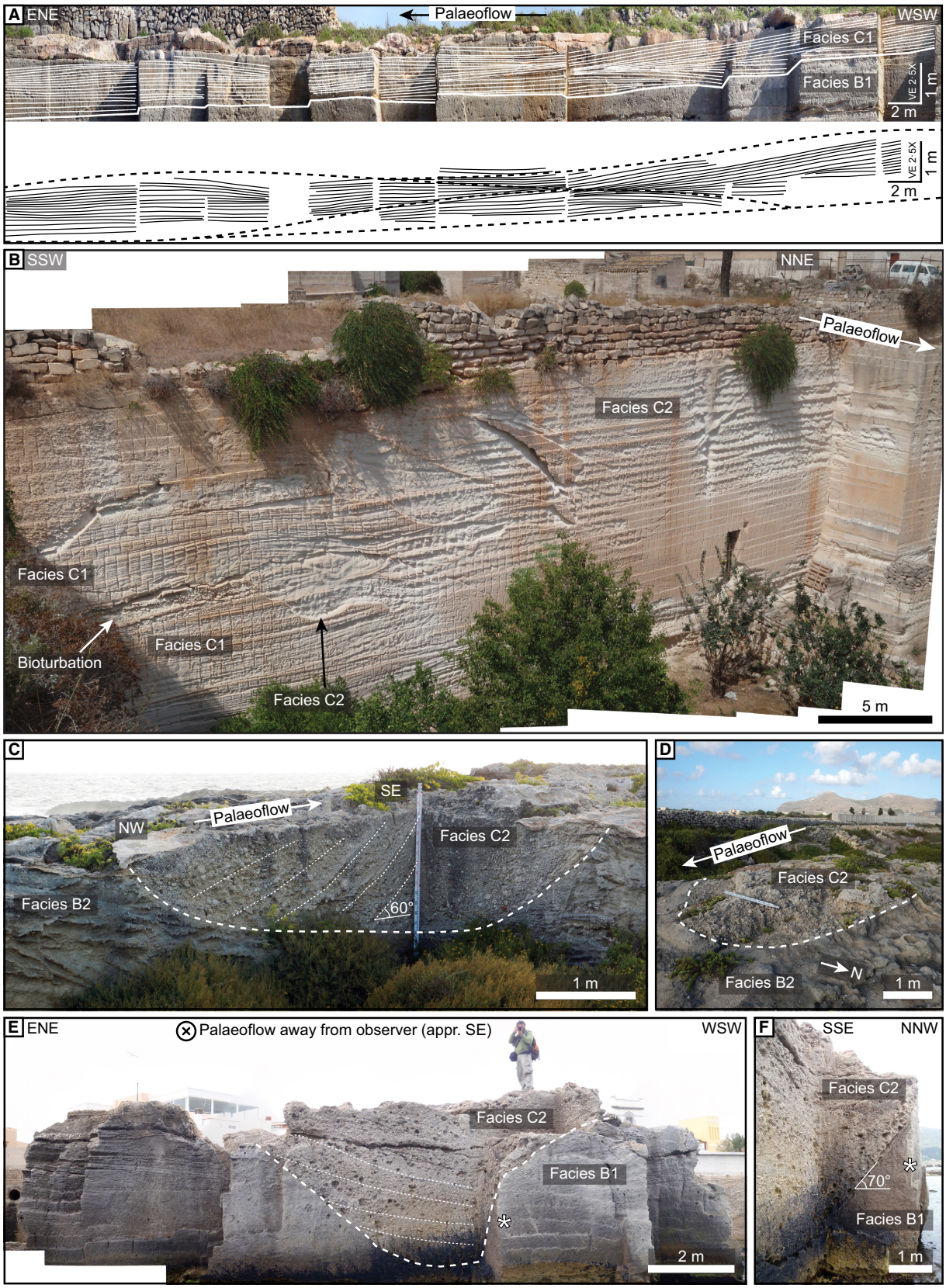
A
ENE
Palaeoflow
WSW
Facies C1
Facies B1
VE 2.5x
1 m
2 m
B
SSW
NNE
Palaeoflow
Facies C2
Facies C1
Bioturbation
Facies C1
Facies C2
5 m
C
SE
NW
Palaeoflow
Facies C2
Facies B2
60°
1 m
D
Palaeoflow
Facies C2
N
Facies B2
1 m
E
ENE
Palaeoflow away from observer (appr. SE)
WSW
Facies C2
Facies B1
2 m
F
SSE
NNW
Facies C2
70°
Facies B1
1 m

Fig. 12. Continued.

to 60°) characterize some fills (Fig. 12C). Cross-beds dip towards the north/north-west, which is opposite to the dip of the master bedding and also opposite to the palaeoflow-indicating cross-beds of FA-B. Facies C2 cross-beds display concave-up geometries, which flatten and straighten upward. In fills with higher proportions of coarse sand and granule-size matrix, internal cross-beds with dips up to 25° resemble the crude and spaced stratification of Facies C1 (Fig. 12G).

Facies C2 cross-beds display long, concave-up basinward terminations, usually consisting of crude stratification that grades into spaced stratification downdip (towards a proximal position). Facies C2 cross-beds are thus more erosional in a proximal position within the fill, reaching a maximum at their lowermost position where cross-beds become progressively less steep, reaching a horizontal tangent in their troughs (Fig. 12G). From this point, cross-beds extend slightly further upstream with opposite dip before being truncated by the overlying cross-bed. The proximal set boundary is thus a composite erosion-surface in which each erosion-based cross-bed is truncated by the succeeding one (Fig. 12H).

Facies C3: Backset-stratified rudstones. The coarse rudstones of Facies C3 occur in Zone II and in particular in Zone III. Composition trends are comparable to Facies C1 and C2, most notably the basinward transition from oysters, *Pecten maximus* and lithoclasts, to spherical rhodoliths ranging from a few to 15 cm in diameter. Bioturbation structures are absent, with the exception of rare, isolated *Ophiomorpha* shafts up to 4 m in length.

Facies C3 constitutes the largest part of thick FA-C units in Zone III, which locally cut deep

into the underlying FA-B (Fig. 4). Also, in Zone II the thickest beds are predominantly composed of Facies C3. Wavy geometries are abundant, forming low-angle to high-angle cross-beds that dip opposite to the master bedding (Fig. 12I). Set boundaries are gradational where Facies C3 is composed of coarse sand to granules, herewith mimicking Facies C1. Set boundaries are progressively more erosional with larger grain size, resembling the scour and fill structures of Facies C2. However, in most exposures Facies C3 consists of distally stacked sets comprising cross-beds dipping opposite to the master bedding, which attain concave-up geometries in their proximal portion and adopt more convex-up shapes towards their basinward end (Fig. 12I). Such 2 to 20 cm thick, sigmoidal cross-beds are locally up to 20 m long, and typically fine and thin basinward, away from the proximal set boundary, showing a longitudinal transition from spaced to crude (and frequently back to spaced) stratification. Sets slightly taper in a basinward direction (Fig. 12I), locally creating lenticular outlines and shingled stacking patterns. At the basinward end of sets, stratification is truncated by the composite erosion surface of the subsequent set, or, where the set boundary is gradational, stratification continues into the adjacent set. Where Facies C3 superposes form sets of Facies B3, the contact shows features similar to boundaries of adjoining Facies C3 sets (Fig. 10E).

The uppermost part of Facies C3 and locally also the deposits overlain by this facies have commonly been affected by recumbent folding (Fig. 13A) and water escape (Fig. 13B to D), the latter leading to flame and dish structures. Intervals disturbed by soft-sediment deformation are locally more than 1 m thick.

Facies C4: Pinching-out planar stratified rudstones. At the basinward termination of FA-C units, the planar stratified rudstones of Facies C4 prevail. The key locality is near the lighthouse at Punta Marsala (Fig. 12J). Facies C4 has characteristics of upper-stage plane bedding, including local primary current lineation (Stokes, 1947; Crowell, 1955), in particular where lamination is of sub-centimetre scale. Where internal stratification is thicker, Facies C4 resembles Facies A1, with the exception of the omnipresent bioturbation structures in the latter, which are absent in Facies C4. Facies C4 occurs in beds that rarely exceed 1 m in thickness and pinch out over distances of up to tens of metres. Locally, such beds display large-scale undulations.

Interpretation

The sigmoidal stratification forming interwoven lenticular sets (Facies C1), conglomeratic scour and fill structures (Facies C2) and distally stacked lenticular sets (Facies C3) dips opposite to the master bedding and opposite to the majority of the palaeoflow-indicating cross-beds of FA-B. Such stratification was deposited dipping in an upstream direction and is therefore backset-bedding (Davis, 1890; Jopling & Richardson, 1966). Backset-bedding is characteristic of upstream-migrating bedforms generated under supercritical flow conditions (Fr > 1) (Kennedy, 1963; Carling & Shvidchenko, 2002; Cartigny *et al.*, 2014). The deposits of FA-C are interpreted as unstable antidunes (Facies C1), chute and pool structures (Facies C2) and cyclic steps (Facies C3) (Fig. 14). The deposits of Facies C4 represent upper-stage plane bedding at the distal termination of FA-C units.

Facies C1: Unstable antidunes. Facies C1 formed by the aggradation of unstable antidunes (Fig. 14A) under high rates of sediment fallout. The concave to convex-up stratification is locally continuous between adjacent sets and shows gradational set boundaries. Where this is not the case, stratification thins and condenses creating apparent onlap onto set boundaries. Only very rarely are set boundaries erosional. This implies that sedimentation occurred also on the lee side of antidunes resulting in their climbing character. Set lengths indicate antidune wavelengths of 20 to 30 m.

Backset beds progressively thicken towards the antidune crest as a result of high rates of suspension fallout, which led to stoss side steepening. This invoked a positive feedback mechanism whereby each subsequent backset bed steepened the antidune stoss side more and more. This induced progressive deceleration and thickening of the flow on the stoss side, which caused a drop of the Froude number over the crest until it ultimately passed the critical threshold of Fr = 1 and the flow became subcritical (see Eq. 1). This involved breaking of the wave and the formation of a weak hydraulic jump on the antidune crest, which surged upstream into the trough of the adjacent antidune (Fig. 14A ②) (Hand, 1974; Alexander *et al.*, 2001; Spinewine *et al.*, 2009; Cartigny *et al.*, 2014).

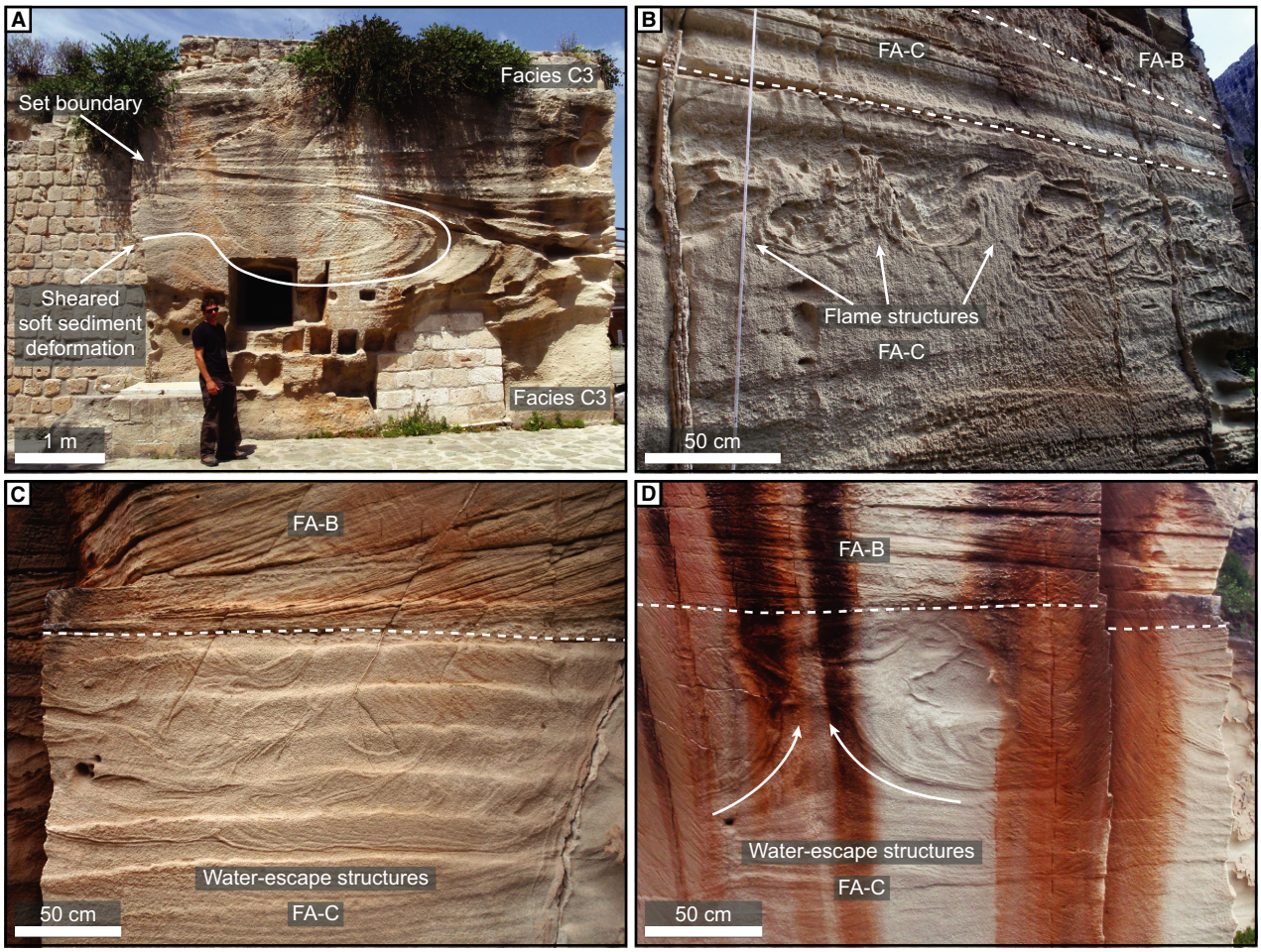

Fig. 13. Soft-sediment deformation structures in Facies Association C. (A) Sheared soft-sediment deformation at the upper part of a Facies C3 set that is overlain by another Facies C3 set of the same unit. The composite erosion-surface (set boundary) between the two sets suggests that the soft-sediment deformation is probably the result of a negative pressure gradient below a hydraulic jump. Cava Sant'Anna (N37·930865° E12·331208°). (B) Flame structures as a consequence of water escape. Fra Santo (N37·921098° E12·361605°). (C) and (D) Water-escape structures in the upper portion of FA-C units. Bue Marino (N37·917260° E12·365796°). Dashed lines indicate unit boundaries.

In experiments (Hand, 1974; Alexander *et al.*, 2001; Cartigny *et al.*, 2014) wave breaking is commonly accompanied by erosion. Here, however, high sediment concentrations induced hindered erosion (Winterwerp *et al.*, 1992) to such an extent that even the supercritical flow was depositional. This prevented the formation of erosional set boundaries. Directly downstream of the transient hydraulic jump that followed the surge, rapid suspension fallout restored the morphological equilibrium between flow and bed by the deposition of backset beds (Fig. 14A ③). The latter are thickest at their upstream side and thin towards the antidune crest, which caused the hydraulic jump to rapidly attenuate until it ultimately flushed downstream (Fig. 14A ④) after which in-phase waves were re-established and supercritical conditions were restored throughout the flow (Fig. 14A ⑤) (Hand, 1974; Alexander *et al.*, 2001; Spinewine *et al.*, 2009; Cartigny *et al.*, 2014).

Unstable antidune deposits are distinguished from cyclic step deposits by more symmetrical geometries (parallel to palaeoflow direction), absence of sharp grain-size breaks, common gradational set boundaries, occurrence in beds that are commonly thinner, stratification that is commonly less thick and less steep, and as a result an amplitude to wavelength ratio that is lower (Table 1).

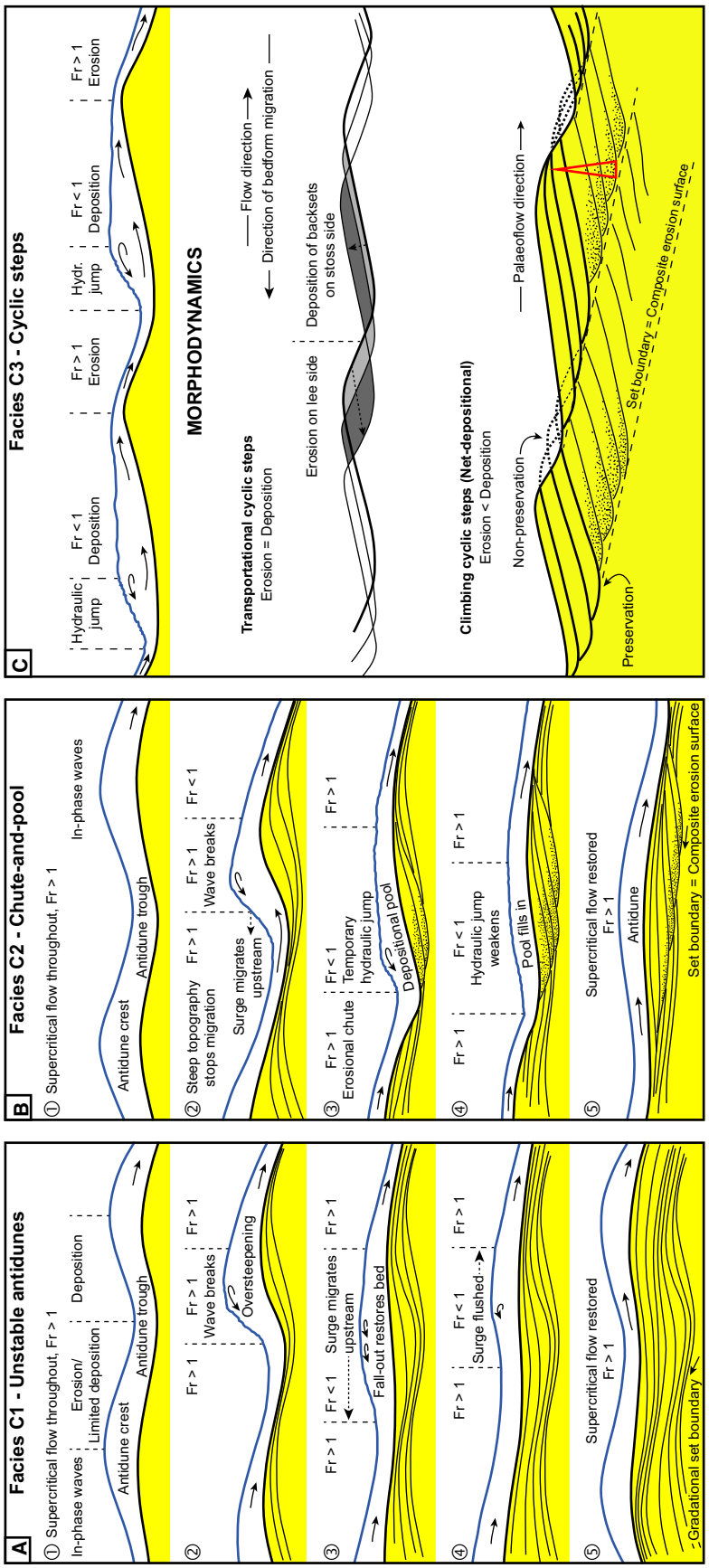

Fig. 14. Interpretation of Facies Association C showing the formation of: (A) wavy stratification of Facies C1 by unstable antidunes under periodically breaking in-phase waves; (B) scour and fill structures of Facies C2 on the stoss side of a chute and pool characterized by the more strongly breaking of in-phase waves and the subsequent formation of a temporary hydraulic jump (HJ); and (C) backset-stratification of Facies C3 by cyclic steps marked by a train of asymmetrical steps overridden by alternating subcritical (Fr < 1) and supercritical (Fr > 1) flow. Red triangle shows the fining-upward trend of sets. These flow dynamics apply to subaerial and submerged flows.

Facies C2: Chute and pool structures. Facies C2 encompasses bio-conglomeratic scour and fill structures that either form stacked sets or occur as isolated bodies up to 10 m long. Such structures are filled with upstream-dipping backset beds that are much steeper than those of Facies C1. Backset beds are erosion-based at their upstream portion where they terminate in the set boundary. Set boundaries thus comprise composite erosion surfaces (amalgamated surfaces and pseudo-foresets of Dietrich *et al.*, 2016) consisting of a series of climbing, spoon-shaped scours that present a diagnostic feature of hydraulic-jump-related deposition (Postma *et al.*, 1983; Nemec, 1990; Massari, 1996). These structures on Favignana Island were previously interpreted as 'cross-bedded channel-fills' (Ślączka *et al.*, 2011). However, three-dimensional geometries and lateral discontinuity (Fig. 12C to F) are not in line with such an interpretation.

The formation of scour and fill structures is closely associated with the unstable antidunes of Facies C1 (Fig. 14B). Flows with greater Froude numbers than the formative flows of unstable antidunes generated antidunes with greater amplitude accompanied by an amplification of the overriding in-phase waves (Kennedy, 1963; Hand, 1974; Alexander & Fielding, 1997; Duller *et al.*, 2008). Progressive stoss-side steepening occurred in a way similar to unstable antidunes. However, enhanced flow thickness over the antidune crest and greater associated velocities resulted in a more abrupt breaking of in-phase waves and the formation of a stronger surge (Fig. 14B ②; Cartigny *et al.*, 2014). The greater morphological imbalance between flow and bed could not be restored by deposition alone, as with unstable antidunes, but required significant erosion while the surge migrated upstream. Surge migration ceased near the trough of the adjacent antidune, where it transformed into a temporary hydraulic jump (Fig. 14B ③; Hand, 1974; Alexander *et al.*, 2001; Cartigny *et al.*, 2014).

Erosion just upstream of the hydraulic jump resulted from high shear stresses at the base of the supercritical incoming flow. Pulsation during scouring created the crude and spaced stratification (Hiscott, 1994; Sohn, 1997; Cartigny *et al.*, 2013), which characterizes FA-C in general. Here, such pulsation triggered the alternation of erosion and deposition generating the composite erosion surface consisting of a series of climbing concave-upward, spoon-shaped scours. Directly downstream of the hydraulic jump, high rates of suspension fallout resulted from the rapid deceleration of the flow and the accompanied decline in basal shear stress (Lennon & Hill, 2006; MacDonald *et al.*, 2009; Cartigny *et al.*, 2014). Continued deposition of progressively less steep backset beds filled the scoured depression, forcing the hydraulic jump to migrate upstream whilst becoming smaller and weaker (Fig. 14B ④) until it was eventually flushed downstream (Hand, 1974; Alexander *et al.*, 2001; Cartigny *et al.*, 2014). The infilling of the scour was thus accompanied by progressively increasing basal shear stresses, which gradually enhanced the ability of the flow to transport coarse material. Therefore, scour and fill structures are commonly fining upward. Grain-size variations in the deposit are thus not a result of changes in the grain-size distribution of the sediment carried within the flow but are due to selective deposition. Grain-size distributions within the formative flows of Facies C1 and C2 were probably very alike.

The irregularity of the lateral sides of scour and fill structures is caused by local, small-scale side-wall collapses below the hydraulic jump due to fluidization (Postma *et al.*, 2009; Turmel *et al.*, 2012; Cartigny *et al.*, 2014; Postma *et al.*, 2014; Dietrich *et al.*, 2016). However, also the pulsating character of the flow, resulting in the alternation of erosion and deposition, may have played a role. The steepness of the side walls, which frequently exceeds the angle of repose of granular material, demonstrates the rapid deposition of backset bedding, which must have been fast enough in stabilising the walls of the erosional depression to prevent their collapse (Massari, 1996; Hansen, 1999).

Stable antidunes in experimental studies (Cartigny *et al.* 2014), related to stable in-phase waves, transform into unstable antidunes characterized by occasional wave breaking around mean Froude numbers of Fr_{50} = 1·1. Flows marked by higher Froude numbers generate unstable antidunes with greater amplitude related to in-phase waves that break more abruptly and subsequently develop into transient hydraulic jumps. Such bed morphologies are referred to as 'chute and pool' structures *sensu* Simons *et al.* (1965) (see also Hand, 1974; Massari, 1996; Fralick, 1999; Alexander *et al.*, 2001; Russell & Arnott, 2003; Duller *et al.*, 2008; Lang & Winsemann, 2013; Cartigny *et al.*, 2014) generating the scour and fill structures of Facies C2. Wave breaking invoked the

formation of powerful, upstream-migrating surges that scoured local erosional depressions. Where surges came to a halt, typically in the trough of the adjacent antidune (Cartigny *et al.*, 2014), temporary hydraulic jumps developed. Rapid suspension fallout directly downstream of the jump resulted in the deposition of partly erosion-based backset-bedding, filling the initial scour and depression between the antidunes until the equilibrium between flow and bed had been restored.

The sedimentary characteristics of chute and pool deposits reflect a hydrodynamic behaviour that is transitional between antidunes and cyclic steps. This is reflected by the common co-occurrence of Facies C1 and C2 (the latter cutting into the former). Compared with antidune deposits, the deposits of chute and pools comprise very steep backset-beds (up to exceeding the angle of repose). Backset-beds are much thicker with bases terminating in the composite erosion surface of the set boundary. These properties are shared with cyclic step deposits. However, while cyclic step deposits commonly consist of regularly stacked sets, the deposits of chute and pools involve isolated bodies (locally irregularly stacked), although both are commonly fining-upward. Chute and pool sets (scour and fill bodies) have thickness to length ratios that are higher than for cyclic step sets and much higher than for antidune sets (Table 1).

Facies C3: Cyclic steps. The distally stacked, lenticular sets of Facies C3 contain wavy backset-bedding, which is convex-up at the basinward end of sets and concave-up at their proximal portions. Set boundaries mimic those of the scour and fill structures of Facies C2, consisting of a series of climbing spoon-shaped scours. Such composite erosion-surfaces are diagnostic to hydraulic-jump-related deposition (cf. the amalgamation surfaces and pseudo-foresets of Dietrich *et al.*, 2016).

Cyclic steps (Parker, 1996) are capable of building such distally stacked sets of backset bedding (Fildani *et al.*, 2006; Kostic & Parker, 2006; Spinewine *et al.*, 2009; Cartigny *et al.*, 2011; Kostic, 2011; Cartigny *et al.*, 2014). These bedforms consist of a series of commonly downstream-asymmetrical steps with hydraulic jumps in the trough at the base of each lee side (Fig. 14C) (Turmel *et al.*, 2015; Zhong *et al.*, 2015; Dietrich *et al.*, 2016; Normandeau *et al.*, 2016; Slootman, 2016; Lang *et al.*, 2017; Vellinga *et al.*, 2018). Erosional, supercritical flow characterizes the steep lee side, at the toe of which rapid deceleration supports the semi-permanent presence of a hydraulic jump (Vellinga *et al.*, 2018) for as long as the bed configuration is maintained (Fagherazzi & Sun, 2003; Sun & Parker, 2005; Taki & Parker, 2005). Directly downstream of the hydraulic jump, rapid suspension fallout from the re-accelerating subcritical flow results in the deposition of backset beds on the stoss side of the bedform (Cartigny *et al.*, 2011; Postma *et al.*, 2014; Vellinga *et al.*, 2018). Lee-side erosion and stoss-side deposition thus lead to the upstream migration of cyclic steps (Fagherazzi & Sun, 2003; Sun & Parker, 2005; Taki & Parker, 2005). The wavy character that marks some backset beds reflects superimposed antidune undulations (Spinewine *et al.*, 2009; Cartigny *et al.*, 2014; Dietrich *et al.*, 2016), although dewatering structures may also create wavy geometries (Slootman, 2016), albeit of more irregular nature.

Deposits reflect the changing character of the flow as it overrides a single step (Postma & Cartigny, 2014; Postma *et al.*, 2014). Directly downstream of the hydraulic jump, shear stresses are of minor importance and deposition (generally coarser-grained) is largely controlled by suspension fallout (Cartigny *et al.*, 2014; Vellinga *et al.*, 2018). Flow thinning and acceleration towards the crest of the bedform gradually replace suspension fallout by traction sedimentation (Postma *et al.*, 2014), depositing preferentially finer material due to the facilitated transport of the coarser fraction under conditions of increased shear stress, a process which is still poorly understood. Individual backset beds thus show a downstream-fining trend (Postma *et al.*, 2014; Dietrich *et al.*, 2016; Vellinga *et al.*, 2018). The upstream migration of cyclic steps, therefore, results in fining-upward Facies C3 sets (Fig. 14C). Backset beds with coarser material are marked by enhanced erosion at the set boundary, suggesting a greater supercriticality of the formative flow down the lee side and a higher intensity of the hydraulic jump. In addition, cyclic steps are three-dimensional features (Postma *et al.*, 2014; Slootman, 2016). As a consequence, cross-sections vary as a function of the orientation with respect to the longitudinal axis of the structure. In a central cross-section, structures tend to be more erosional than in a cross-section that dissects the lateral extremity of a Facies C3 set.

Soft sediment deformation structures in Facies C3 are the result of rapid deposition and, consequently, incorporation of large amounts of pore water between grains (Postma *et al.*, 2009; Cartigny *et al.*, 2014). Rapid burial of such water-oversaturated deposits induced the upward escape of water as sediments became more densely packed, squeezing out the excess pore fluid. Shear stresses exerted by the formative flow played an important role in the formation of associated recumbent folding (Fig. 13A). Water escape may be enhanced by the reduced pressure below hydraulic jumps, inducing a negative pressure gradient in favour of the upward migration of pore water (Postma *et al.*, 2009).

Cyclic step deposits are distinguished from antidune deposits by sets that commonly have sharp grain-size breaks at erosional set boundaries. Cyclic step sets fine downstream and upward and are more asymmetrical than antidune deposits as expressed by stratification that almost exclusively dips upstream and is commonly thicker than for antidunes. Although changes in flow conditions may hamper the formation of very regularly stacked sets (separated by composite erosion surfaces), cyclic step deposits do not form isolated scour and fill bodies like chute and pools do. Cyclic step sets have higher amplitude to wavelength ratios than antidune sets (Table 1).

Facies C4: Pinching-out upper-stage plane bedding. Facies Association C units pinch-out over as little as 100 m. Associated deposits are composed largely of Facies C4, consisting of centimetre to millimetre-scale planar stratification. Local primary current lineation suggests deposition under upper-stage plane bed conditions. Some Facies C4 beds contain large-scale undulations mimicking slightly aggradational antidune stratification. Rapid dissipation of flow energy towards clinoform toe sets, by the attenuation of the gravitational driving force, induced the deposition of upper-stage plane bedding under waning flow conditions.

Facies Association D: Subcritical-flow strait deposits

Description

Facies D1: Bryozoan-rich compound cross-bedded rudstones and grainstones/packstones. Facies Association D consists of Facies D1 alone, comprising dark yellow to orange rudstones and grainstones to packstones (Fig. 15A) occurring exclusively in Zone IV in the south-eastern part of the study area (Fig. 1). The bulk of Facies D1 is composed of coarse sand to granule-size bioclasts. However, much coarser biogenic material occurs in the basal parts of trough cross-beds and in lags between compound cross-beds (Fig. 15B). Such outsized fragments include macrofossils like articulated pectinids, intact echinoderms, delicate bryozoan frameworks and, more rarely, rhodoliths (Fig. 15C and D). Grainstones and packstones are commonly *Thalassinoides*-bioturbated, whereas rudstones are not.

In terms of sedimentary structures, grain-size distribution and composition, Facies D1 is largely similar to Facies B2, containing the remains of coralline red algae, echinoderms, bivalves, large benthic foraminifera and bryozoans. Bryozoans occur in significantly higher abundance in Facies D1 than in Facies B2, at the cost of red algae (Fig. 7). Lithoclasts are absent in Facies D1. Fines are present in the matrix of all packstones and some rudstones in variable proportions, comparable to Facies B1. There is no marked difference in mineralogy or bulk rock chemistry that differentiates Facies D1 from FA-B and FA-C (Slootman, 2016).

Facies D1 is cross-bedded in a way similar to Facies B2 (Fig. 15A), consisting of sets and cosets composed mostly of southward-dipping compound cross-beds with abundant reactivation surfaces. Compound cross-beds are up to 50 cm thick, the majority not exceeding 20 cm. Typically, they dip less than 20° and consist of decimetre-scale trough cross-bedding. Compound cross-beds comprise 1 to 3 m thick sets, which are vertically stacked into cosets up to 15 m thick. The dip of the highest order cross-bedding is widely variable in almost all directions yet dips predominantly towards the north and south (Fig. 8). In contrast to Facies B2, the compound cross-bedding of Facies D1 commonly dips northward. This is most striking where Facies D1 sets abut southward-dipping compound cross-beds of Facies B2 at the transition from Zone III to Zone IV (Fig. 5). Here, two types of northward-terminating Facies D1 sets are observed: (i) form sets, up to 2 m thick, of northward-migrating composite dunes covered by Facies B2 at their lee side, preserving the outlines of the formative bedforms; and (ii) semi-lenticular sets, up to 2 m thick, with concave-up bases, resting in decametre-wide depressions at the top of FA-C. Accumulations of the 'Boreal Guest' bivalve *Arctica islandica* (Raffi, 1986),

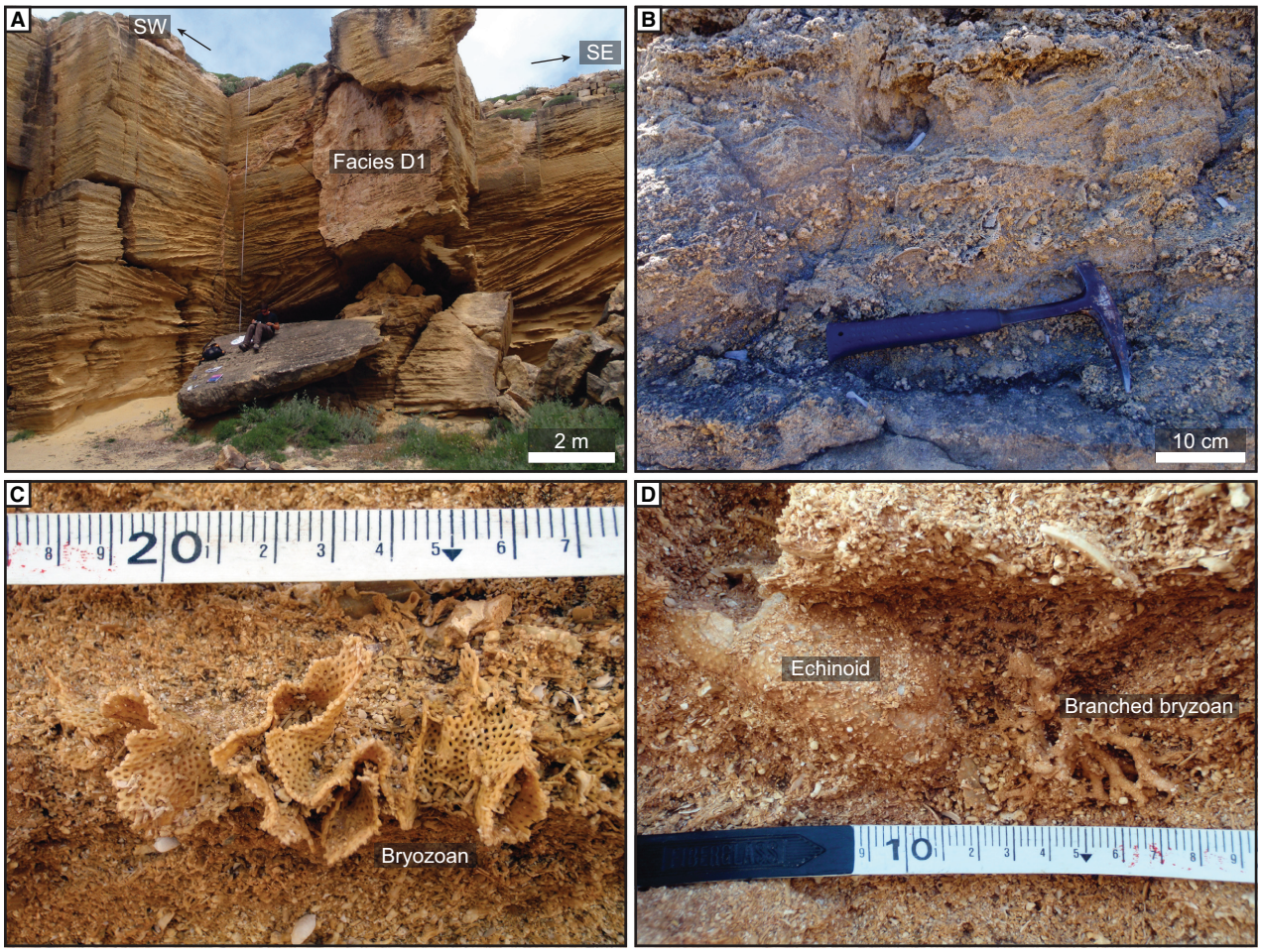

Fig. 15. Facies Association D in Zone IV (offshore environment). (A) Dark yellow to orange, bryozoan-rich rudstones, grainstones and packstones of FA-D marked by compound cross-bedding with variable dip directions (see rose diagrams in Fig. 8) reflecting their formation by composite dunes in an offshore setting that was occasionally affected by currents of variable direction. Bue Marino (N37·917544° E12·369715°). Facies Association D contains a high proportion of outsized skeletal components such as: (B) red algae debris; (C) delicate bryozoans; and (D) echinoids and rare branched bryozoan fragments. Measuring tape in (C) and (D) shows centimetres.

some articulated, occur at the distalmost position of the study area (Cala Azzurra).

Interpretation

Facies D1 reflects deposition in an environment beyond the extension of the prograding clinoforms, which was deeper than for FA-B on the basis of skeletal composition (more bryozoans at the cost of red algae). Facies D1 originated by the predominantly southward migration of composite dunes on the shelf floor, which formed by the lateral stacking of decimetre-scale parasitic bedforms. This mechanism is similar to that of Facies B2. In the absence of intervals consisting of other facies, such as FA-C units in between FA-B, stacking of Facies D1 sets produced up to 15 m thick cosets (Fig. 15A). The widespread presence of fines within Facies D1 packstones suggests periods of quiescence marked by settling and infiltration of fines into sea-floor sediments. Additional evidence is provided by macrofossil accumulations in between or within Facies D1 compound cross-beds. Similar to the lags in FA-B these fossils represent the remains of *in situ* benthic organisms such as bivalves, echinoderms and delicate bryozoans.

The abundance of reactivation surfaces within compound cross-beds suggests that Facies D1 formed through numerous events of subcritical flow. Although unidirectional flow prevailed during individual events, flow direction was variable between successive events. Currents

were predominantly directed towards the north or south (i.e. slope-parallel) and also affected some decimetre-scale dunes in the toe sets of FA-B. Here, smaller-scale dunes were not capable of generating metre-scale composite dunes, most likely because the sea floor exceeded the critical slope for the upslope migration of larger bedforms. Distal of the toe of slope, however, the sea floor was sufficiently near-horizontal to allow the formation of northward-migrating composite dunes. Although in a minority, northward-migrating composite dunes formed extensive sets many tens of metres long, attesting that they could migrate northward for as long as the sea floor was sufficiently flat. Upon reaching a clinoform toe set at the Zone III to IV transition, the southward-dipping sea floor exceeded the threshold slope for upslope migration, forcing northward-migrating Facies D1 composite dunes to terminate there. Alternatively, such dunes were buried by southward-migrating dunes of FA-B, preserving a Facies D1 dune form set (Fig. 5). The relevance of the bivalve *Arctica islandica* at the base of some of the youngest FA-D beds lies in the fact that this Boreal species colonized the Mediterranean during cold periods in the Early Pleistocene (Raffi, 1986; Di Geronimo *et al.*, 2000; Pedley & Grasso, 2006).

DISCUSSION

Evolution of a carbonate delta

The Pleistocene cool-water carbonate wedge of Favignana Island is interpreted as a *carbonate delta* (Fig. 16A), which is a sediment body in the lee of a submerged sill covered by skeletal debris in a shallow-marine gateway between two topographic highs. The carbonate delta formed by deposition from expanding currents that were funnelled through the shallow-marine gateway (similar to the carbonate delta drift of Lüdmann *et al.*, 2018), while beach environments surrounded Favignana palaeo-island (Facies Association A, Zone I). The Favignana platform itself is not preserved, although its former existence between the two palaeo-islands is inferred from the prograding clinoforms, which were identified as platform-slope deposits. These clinoforms went through an initial aggradation (Zone II) and subsequent progradation phase (Zone III). The carbonate delta prograded for several kilometres eastward into a strait on the Sicily Shelf between the two palaeo-islands on one side and Sicily mainland on the other. In the strait, bryozoan-dominated skeletal sediment was reworked by north–south slope-parallel currents into large subaqueous composite dunes (Facies Association D, Zone IV) which interdigitated with the toe of slope of the carbonate delta (Fig. 16A). Some cross-bedded carbonate deposits in other straits were interpreted as the product of subaqueous dunes of tidal origin (Anastas *et al.*, 1997; Longhitano, 2011, 2013; Reynaud *et al.*, 2013; Rossi *et al.*, 2017). There are, however, examples of cross-bedded carbonate deposits that formed in the absence of tidal currents (Betzler *et al.*, 2006; Puga-Bernabéu *et al.*, 2010). Although tidal signatures were not observed in the Favignana carbonate delta nor in the strait deposits of FA-D, tidal reworking in the strait cannot be excluded with certainty.

Removal of skeletal debris off the platform in the shallow-marine gateway between the two palaeo-islands sourcing the carbonate delta, took place by two types of episodic event; Froude-subcritical and supercritical flows, which yielded the bimodal facies stacking pattern of the Favignana carbonate wedge. Subcritical currents generated subaqueous dunes (Facies Association B; 52% of platform-slope deposits; Fig. 4). Supercritical flows associated with in-phase waves and hydraulic jumps formed upper-flow-regime bedforms such as antidunes, chute and pools and cyclic steps (Facies Association C; 48% of platform-slope deposits).

The episodic nature of subaqueous dunes is evidenced by intense bioturbation and colonization of the bed by macrofauna such as echinoids and bivalves during long periods in which there were no currents down the carbonate slope. Based on numerous reactivation surfaces, different degrees of bioturbation and variation in the thickness of compound cross-beds and sets, Slootman *et al.* (2016a) estimated that around 50 to 500 events together generated a single FA-B clinoform unit. A deflection to the right of FA-B cross-beds with respect to the slope gradient may have been introduced by axis-parallel currents in the strait such as observed elsewhere (Longhitano & Steel, 2017; Michaud & Dalrymple, 2016; Rossi *et al.*, 2017), although Coriolis deflection (to the right on the Northern Hemisphere) cannot be excluded (Puga-Bernabéu *et al.*, 2010).

The absence of bioturbation and the lateral continuity of the anomalously thick FA-C beds suggest that FA-C units were deposited during single events with average sedimentation rates one to two orders of magnitude greater than

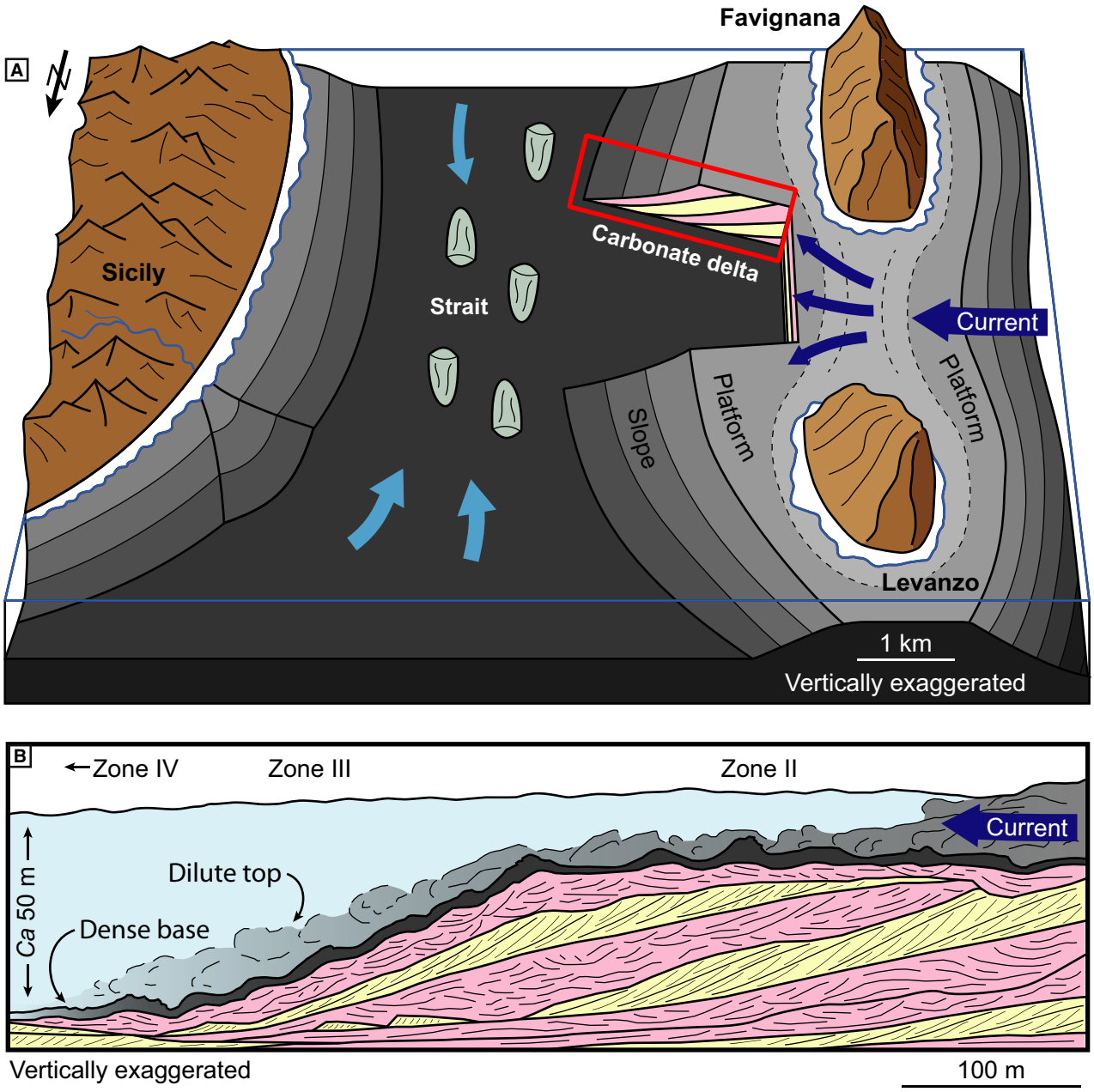

Fig. 16. (A) Conceptual deposition model and (B) cross-section showing a supercritical turbidity current with a high-density basal part that generates bedforms. Continued deposition of subaqueous dunes and turbidity-current deposits led to the formation of a carbonate delta, which today is exposed as the Favignana carbonate wedge.

FA-B events. Antidune wavelength enables the reconstruction of flow properties during FA-C events (Hand, 1974) by:

$$U = \sqrt{\frac{gL}{2\pi}\frac{\rho_{\text{flow}} - \rho_{\text{amb}}}{\rho_{\text{flow}} + \rho_{\text{amb}}}} \qquad (3)$$

where U is flow velocity, g is gravitational acceleration, L is antidune wavelength (20 to 30 m; for example, Fig. 12A) and ρ_{flow} and ρ_{amb} are the densities of the flow and the ambient medium, respectively. In the case of free-surface flows, the density of air can be neglected and $(\rho_{\text{flow}} - \rho_{\text{amb}})/(\rho_{\text{flow}} + \rho_{\text{amb}}) = 1$. For free-surface flows this yields a velocity of $U = 5{\cdot}6$ to $6{\cdot}8$ m sec^{-1}. In-phase waves overriding unstable antidunes start to break at Fr = 1·1, which would imply a flow thickness of $d = 2{\cdot}6$ to $3{\cdot}9$ m (Eq. 1). Antidune

structures occur everywhere in the slope environment, down to several tens of metres below sea level, evidenced by clinoforms up to 50 m high. This conflicts with the calculated values assuming free-surface flows.

The alternative to free-surface flows are turbidity currents. The antidune structures are composed of spaced stratification (Hiscott, 1994), which was experimentally demonstrated to develop in sediment concentrations of 5 to 15% by volume (Cartigny *et al.*, 2013). The density of the flow is a direct function of sediment concentration. Using ρ_{sed} = 2700 kg m^{-3} for the density of skeletal sediment and Eqs 1 to 3, a turbidity current generating unstable antidunes of 20 to 30 m in wavelength would have had a velocity of U = 1·1 to 2·3 m sec^{-1} and a thickness of 1·4 to 2·2 m, which seem plausible values.

Sediment flux calculations and strontium isotope stratigraphy by Slootman *et al.* (2016a) revealed that subcritical flow events lasted hours to days, recurring every tens to hundreds of years, whereas the supercritical turbidity currents did not exceed a few hours in duration, and occurred on average only once every 14 to 35 kyr. These parameters led these authors to suggest that FA-B formed as the result of wind-induced currents during major storms, while thick FA-C beds were deposited by major turbidity currents that formed due to rare, extreme tsunamis raging over the carbonate platform and delivering vast amounts of skeletal debris to the platform slope (Fig. 16B).

Ascribing storm events to FA-B and tsunamis to FA-C is supported by the composition of biogenic components. Pedley & Grasso (2002) demonstrated that the biodiversity of cool-water carbonates is controlled by water depth. Shallow waters are dominated by the remains of red algae, which are progressively replaced by bryozoan fragments with increasing water depth as the result of *in situ* production. The bryozoan/red algae ratio of FA-B is on average two times higher than that of FA-C (Fig. 7). This implies that the skeletal material of FA-B was on average produced at greater water depths than the sediment of FA-C. Because biogenic composition was measured from platform-slope deposits in all cases, differences in the bryozoan/red algae ratio therefore reflect variations in the relative contribution of *in situ* skeletal production, which was more important for FA-B than for FA-C. The shallow-water signature of FA-C is in line with events associated with the catastrophic erosion of the platform.

Types of carbonate delta

The sediment bodies defined by Lüdmann *et al.* (2018) and named *carbonate delta drift* formed under the influence of persistent currents concentrated over a carbonate-sediment-covered submarine high between islands in the Maldives. This generated persistent point-sourced underflows that built elongated and lobe-shaped channelized sediment bodies attached to a gateway. Despite similarities in topographic setting between the Maldivian example and the Favignana carbonate wedge, there are significant differences. The Favignana sediment body is wedge-shaped and blanket-like, formed by line-sourced discontinuous currents of episodic nature. Therefore, available terminology needs to be extended.

Although the term *delta* is associated with sediment accumulations that develop where rivers enter large bodies of water, the occurrence of deltas is not exclusive to those environments. In the sense that sediment accumulates downstream of a gateway by deposition from expanding currents that are funnelled through a passage, carbonate deltas are analogous to tidal deltas (Sha & de Boer, 1991; Elias & Van der Spek, 2006). The more generic term *carbonate delta* is not in conflict with the terminology of Lüdmann *et al.* (2018), who added *drift* to indicate that the sediment body formed under persistent flow conditions in their case (see also Eberli *et al.*, 2019).

The addition of a shape description using the terminology of Mullins & Cook (1986) would clarify the distinction between the different types of carbonate delta. The supplementary term *fan* can be added for a point-sourced, elongated and channelized carbonate delta, whereas adding the term *apron* is optional to indicate a line-sourced, wedge-shaped and blanket-like body. In this classification, the sediment body of Lüdmann *et al.* (2018) would be a *carbonate delta drift-fan* and the Favignana wedge studied here would be a *carbonate delta apron*. However, both examples can be referred to using the more generic term *carbonate delta* to indicate a sediment body formed by deposition from expanding currents in the lee of a relatively shallow sill that is covered by carbonate sediment and which is affected by sediment removal due to funnelling of currents.

Sequence stratigraphy

The dynamics of cool-water carbonates are closely tied to variations in relative sea level.

Hence, facies suites with characteristic deposition styles (systems tracts) are linked to specific phases of the sea-level cycle (Catuneanu, 2006). Clinoform successions, typically encompassing the most voluminous portion of cool-water carbonate accumulations, are commonly attributed to falling sea-levels and periods of sea-level lowstand (Hansen, 1999; Pedley & Grasso, 2002, 2006; Massari & Chiocci, 2006; Puga-Bernabéu *et al.*, 2010; Massari & D'Alessandro, 2012). During these stages, sediment supply outpaces vertical accommodation space, forcing the system to prograde. However, lack of accommodation space may also result from sea-level stillstand such as during the Early Pleistocene (Pedley & Grasso, 2002) on the condition that sediment production is not switched off. A shutdown of the carbonate factory due to relative sea-level rise is a common scenario for tropical carbonate deposition systems (platform drowning; see review in Schlager, 2005) caused by the sea floor moving out of the photic zone and therewith below the critical threshold for photozoan organisms (James, 1997). A stop in the production of cool-water carbonates as a result of sea-level rise, however, is unlikely because heterozoan organisms largely are not light-dependent (James, 1997).

The Favignana carbonate wedge was dated between 1·6 ± 0·1 Ma and 1·1 ± 0·1 Ma, covering some 500 ± 200 kyr (Slootman *et al.*, 2016a). This period coincides with the fourth-order Emilian highstand (Fig. 17) (Pedley & Grasso, 2002), which is recognized in numerous successions in Sicily and southern Italy (Butler *et al.*, 1997; D'Alessandro & Massari, 1997; Massari *et al.*, 1999; Pomar & Tropeano, 2001; Pedley *et al.*, 2001; Pedley & Grasso, 2002) and elsewhere in the Mediterranean region (Lykousis, 1991; Poole & Robertson, 1991; Hanken *et al.*, 1996; Hansen, 1999). The Emilian is a sub-stage of the Calabrian Stage of the Early Pleistocene (Mauz, 1998; Gibbard & Cohen, 2016). The Emilian highstand is sandwiched between the lowstands of the Santernian and Sicilian Substages (Fig. 17A) (Pedley & Grasso, 2002).

Carbonate production on the platform commenced during the Santernian sea-level rise (Fig. 17B; Slootman *et al.*, 2016a). The transgression led to aggradation accompanied by steepening of the platform slope (Fig. 17C). When the rate of sea-level rise decreased and vertical accommodation space attenuated, the deposition style shifted from aggradation to progradation (Fig. 17D). At the time of full Emilian highstand conditions, the decametre-scale thick wedge that had accumulated started to prograde eastward onto the shelf floor between the palaeo-islands and Sicily. Carbonate production took place everywhere on the sea bed, with the largest area (and most likely also the largest production per unit surface area) located on the platform. Excess skeletal material was occasionally transported towards the platform edge and carried off by migrating composite dunes during subcritical storm-induced currents (FA-B) and, much less frequently, by high-energy turbidity currents that followed the sweeping of huge amounts of skeletal debris during tsunamis (FA-C). Clinoform progradation was contemporary with the activity of subaqueous dunes in the strait on the Sicily Shelf between the palaeo-islands at one side and Sicily mainland at the other (FA-D) due to slope-parallel bottom currents, which were occasionally incorporated within the toe sets of the carbonate delta. The well-established stillstand conditions during the fourth-order highstand that prevailed throughout the Emilian episode lasted several hundred kyr (Pedley & Grasso, 2002; Slootman *et al.*, 2016a). Carbonate production ceased towards the lowstand conditions of the Sicilian Substage.

The Early Pleistocene was subject to high-frequency (fifth-order) glacio-eustatic sea-level fluctuations attributed to the 41 kyr obliquity cycle (Wornardt & Vail, 1991; Catalano *et al.*, 1998). In Sicily and southern Italy, such fluctuations resulted in the formation of carbonate wedges with comparable sequence stratigraphic architectures to the Favignana carbonate wedge (Catalano *et al.*, 1998; Pedley & Grasso, 2002; Massari & Chiocci, 2006; Massari and D'Alessandro, 2012). Where erosion during lowstand conditions was important, only the clinoform successions were preserved. Such prograding carbonate wedges (examples cited above) occur in up to six-storey stacks typically alternating with offshore marls. This raises the question: why did only one thick, fourth-order wedge form on Favignana during a period in which high-frequency sea-level fluctuations resulted in multiple (albeit less extensive) fifth-order stacks in Sicily and southern Italy?

Key to understanding the absence of a high-frequency (fifth-order) sea-level signal is the amplitude of such glacio-eustatic fluctuations with respect to the depth of the depositional environment. Sea-level change is 'felt' most dramatically by sea floors that experience a shift from below storm wave base to above and *vice*

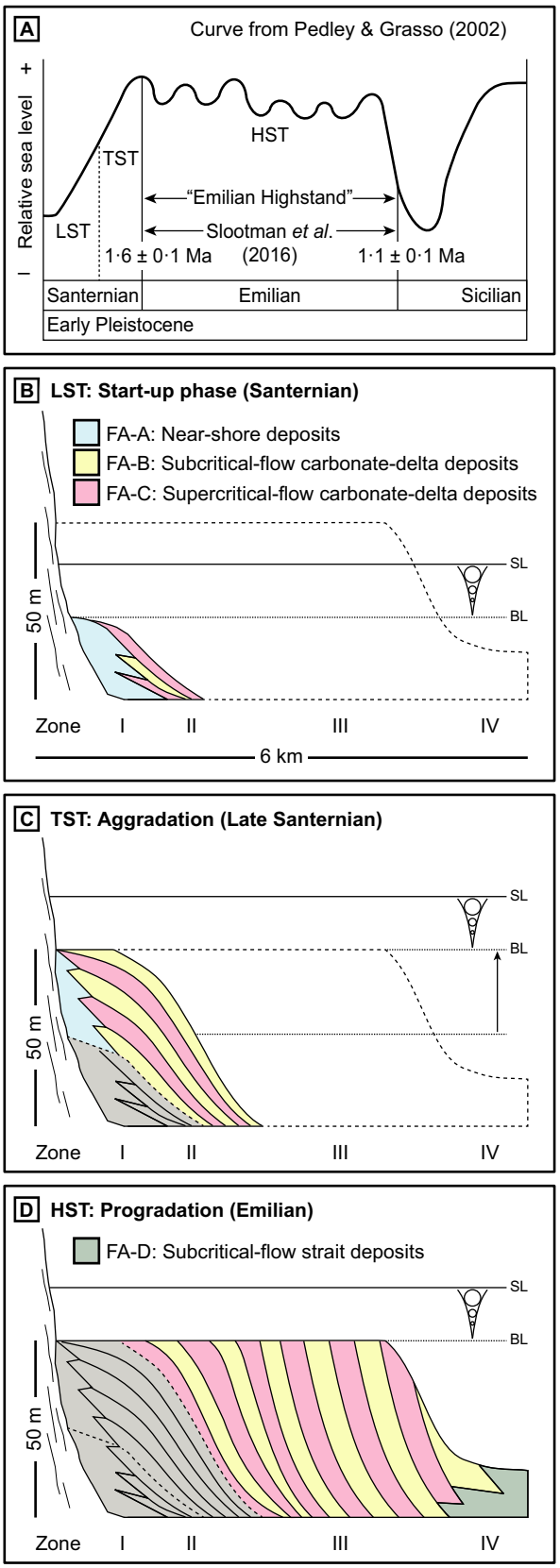

Fig. 17. Sequence stratigraphy of the Favignana carbonate delta. (A) Relative sea-level curve for the Early Pleistocene, emphasising the Emilian highstand. Redrawn after Pedley & Grasso (2002). Schematic evolution of system tracts during the (B) Santernian, (C) Late-Santernian and (D) Emilian. Note extreme vertical exaggeration. LST = lowstand systems tract; TST = transgressive systems tract; HST = highstand systems tract.

versa. Therefore, a sea-level drop of a magnitude comparable to the water depth minus the depth of the wave base is required before sea-floor sediment becomes physically affected by wave-related turbulence. However, when the sea bed is always below hydrodynamic base-level and the system is continuously in catch-up mode, accommodation space will invariably exceed the volume of the skeletal material produced. Such a situation is conceivable only with low vertical accumulation rates and low-amplitude sea-level oscillations. The incidental, although regular, off-ramp transport of sediment by wind and tsunami-induced currents could have caused the bed to be built at maximum up to storm wave base. Funnelling of currents and the associated focusing of energy on the platform may have been pivotal to reaching such conditions.

Pedley & Grasso (2002) estimated the amplitude of the fourth-order Emilian eustatic event at a maximum of 80 m. These authors related six clinoformed carbonate wedges in south-eastern Sicily to superimposed higher-order sea-level variations, each suggested to be of the order of 10 to 30 m. Such relatively low-amplitude sea-level oscillations were of only minor influence on the platform. Pedley & Grasso (2002) further noted that the high-sea-level excursion lasted *ca* 550 kyr, with the fourth-order highstand (still-stand) extending over the entire Emilian Substage (*ca* 1·5 to 1·2 Ma), coinciding with the ages of Slootman *et al.* (2016a). No suggestion was made to explain the origin of the high-frequency perturbations which, given the average duration, might indeed be the 41 kyr glacio-eustasy obliquity cycle (Catalano *et al.*, 1998).

The early Sicilian global sea-level fall at the termination of the Emilian was inferred to have been very rapid and to be associated with a transition from temperate interglacial conditions (Pedley & Grasso, 2006), comparable to the present-day eastern Mediterranean Sea, to much

cooler conditions (Di Geronimo *et al.*, 2000; Pedley & Grasso, 2002, 2006). Such cooling is demonstrated by the Mediterranean colonization of the Boreal bivalve *Arctica islandica*, reflecting conditions similar to those in the present-day southern North Sea with winter temperatures below 9°C (Raffi, 1986). The presence of *Arctica islandica* was interpreted to mark the termination of the Emilian carbonate sequence in south-eastern Sicily (Di Geronimo *et al.*, 2000). Similarly, *Arctica islandica* at the base of the youngest FA-D units on Favignana Island indeed support the shutdown of the carbonate factory (cf. Pedley & Grasso, 2006).

CONCLUSIONS

Carbonate deltas are formed by sediment being carried basinward off of a carbonate platform by funnelling through a shallow-marine gateway between topographic highs. This study describes and interprets the accumulation of the Lower Pleistocene Favignana carbonate delta in the lee of a submarine sill between two islands in the Aegadi Archipelago, building out into a larger strait between the two islands on one side and Sicily on the other. Bedform dynamics on the carbonate delta reveal two types of incidental currents affecting the platform in the gateway: (i) dilute subcritical currents leading to the formation of subaqueous dunes; and (ii) sediment-laden supercritical turbidity currents generating upper flow-regime bedforms including antidunes, chute and pools and cyclic steps. The two types of current invoked a bimodal stacking pattern of clinoform units prograding from the gateway onto a shelf, forming a 50 m high and 6 km long carbonate delta during the Emilian sea-level highstand (1·6 Ma to 1·1 Ma). This study emphasises that the adequate identification of sedimentary structures is essential to the development of sound deposition models. The concept of carbonate deltas, in particular in the light of recent advances in the understanding of supercritical-flow processes, opens the door for revisiting certain carbonate accumulations that were previously interpreted using more classical models.

ACKNOWLEDGEMENTS

This work was performed in the framework of a PhD research project (AS) generously funded by the Department of Public Instruction of the Canton of Geneva, Switzerland. The Société de Physique et d'Histoire Naturelle de Genève is thanked for providing a Bourse Augustin Lombard Fund to AS. This paper benefited from discussions with Joris Eggenhuisen, George Postma, Age Vellinga, Jérémy Ragusa, Jort Koopmans and Robert Kil. Jort Koopmans, Kim Ménage and Jason Nede are thanked for their assistance during field campaigns. Antonietta Rosso is acknowledged for the identification of the 'false coral' fragment in Fig. 15D. We thank Associate Editor Gregor Eberli, Jörg Lang and four anonymous reviewers for their helpful and constructive comments that greatly improved the quality of the manuscript.

REFERENCES

Abate, B., **Incandela, A.** and **Renda, P.** (1997) *Carta Geologica delle Isole di Favignana e Levanzo*. University of Palermo, Dipartimento Di Geologia.

Alexander, J. and **Fielding, C.** (1997) Gravel antidunes in the tropical Burdekin River, Queensland, Australia. *Sedimentology*, **44**, 327–337.

Alexander, J., **Bridge, J.S.**, **Cheel, R.J.** and **Leclair, S.F.** (2001) Bedforms and associated sedimentary structures formed under supercritical water flows over aggrading sand beds. *Sedimentology*, **48**, 133–152.

Allen, J.R.L. (1982) *Sedimentary Structures, Their Character and Physical Basis*. Developments in Sedimentology, 30A. Elsevier, Amsterdam, 593 pp.

Anastas, A.S., **Dalrymple, R.W.**, **James, N.P.** and **Nelson, C.S.** (1997) Cross-stratified calcarenites from New Zealand: subaqueous dunes in a cool-water, Oligo-Miocene seaway. *Sedimentology*, **44**, 869–891.

Ashley, G.M. (1990) Classification of large-scale subaqueous bedforms: a new look at an old problem. *J. Sed. Res.*, **60**, 160–172.

Betzler, C., **Brachert, T.C.**, **Braga, J.C.** and **Martin, J.M.** (1997) Nearshore, temperate, carbonate depositional systems (lower Tortonian, Agua Amarga Basin, southern Spain): implications for carbonate sequence stratigraphy. *Sed. Geol.*, **113**, 27–53.

Betzler, C., **Braga, J.C.**, **Martín, J.M.**, **Sánchez-Almazo, I.M.** and **Lindhorst, S.** (2006) Closure of a seaway: stratigraphic record and facies (Guadix Basin, southern Spain). *Int. J. Earth Sci. (Geol. Rundsch.)*, **95**, 903–910.

Betzler, C., **Braga, J.C.**, **Jaramillo-Vogel, D.**, **Roemer, M.**, **Huebscher, C.**, **Schmiedl, G.** and **Lindhorst, S.** (2011) Late Pleistocene and Holocene cool-water carbonates of the Western Mediterranean Sea. *Sedimentology*, **58**, 643–669.

Brasier, M.D. (1975) An outline history of seagrass communities. *Palaeontology*, **18**, 681–702.

Butler, R.W.H., **Grasso, M.**, **Gardiner, W.** and **Sedgeley, D.** (1997) Depositional patterns and their tectonic controls within the Plio-Quaternary carbonate sands and muds of onshore and offshore SE Sicily (Italy). *Mar. Petrol. Geol.*, **14**, 879–892.

Carling, P.A. and **Shvidchenko, A.B.** (2002) A consideration of the dune: antidune transition in fine gravel. *Sedimentology*, **49**, 1269–1282.

Cartigny, M.J.B., **Postma, G.**, **Van den Berg, J.H.** and **Mastbergen, D.R.** (2011) A comparative study of sediment waves and cyclic steps based on geometries, internal structures and numerical modeling. *Mar. Geol.*, **280**, 40–56.

Cartigny, M.J.B., **Eggenhuisen, J.T.**, **Hansen, E.W.** and **Postma, G.** (2013) Concentration-dependent flow stratification in experimental high-density turbidity currents and their relevance to turbidite facies models. *J. Sed. Res.*, **83**, 1046–1064.

Cartigny, M.J.B., **Ventra, D.**, **Postma, G.** and **Den Berg, J.H.** (2014) Morphodynamics and sedimentary structures of bedforms under supercritical-flow conditions: new insights from flume experiments. *Sedimentology*, **61**, 712–748.

Catalano, R., **Di Stefano, P.**, **Sulli, A.** and **Vitale, F.P.** (1996) Paleogeography and structure of the central Mediterranean: sicily and its offshore area. *Tectonophysics*, **260**, 291–323.

Catalano, R., **Di Stefano, E.**, **Sulli, A.**, **Vitale, F.P.**, **Infuso, S.** and **Vail, P.R.** (1998) Sequences and systems tracts calibrated by high resolution bio-chronostratigraphy: the central Mediterranean Plio-Pleistocene record. In: *Mesozoic and Cenozoic Sequence Stratigraphy of European Basins* (Eds J. Hardenbol, J. Thierry, M.B. Farley, T. Jacquin, P.C. De Graciansky and P. Vail), *SEPM Spec. Publ.*, **60**, 155–177.

Catalano, R., **Merlini, S.** and **Sulli, A.** (2002) The structure of western Sicily, central Mediterranean. *Petrol. Geosci.*, **8**, 7–18.

Catuneanu, O. (2006) *Principles of Sequence Stratigraphy*. Elsevier, Amsterdam, 386 pp.

Cheel, R.J. (1990) Horizontal lamination and the sequence of bed phases and stratification under upper-flow-regime conditions. *Sedimentology*, **37**, 517–529.

Chow, V.T. (1959) *Open-channel Hydraulics*. McGraw-Hill Book, New York, NY. 679 pp.

Crowell, J.C. (1955) Directional-current structures from the Prealpine Flysch, Switzerland. *Geol. Soc. Am. Bull.*, **66**, 1351–1384.

D'Alessandro, A. and **Massari, F.** (1997) Pliocene and Pleistocene depositional environments in the Pesculuse area (Salento, Italy). *Riv. Ital. Paleontol. Stratigr.*, **103**, 221–258.

D'Angelo, S., **Catalano, R.**, **Mancuso, M.**, **Agate, M.**, **Lo Cicero, G.**, **Sulli, A.**, **Bornati, P.**, **Lo Iacono, C.**, **Lucido, M.**, **Di Maio, D.**, **Macaluso, T.**, **Di Stefano, P.**, **Frixa, A.**, **Gugliotta, C.**, **Fallo, L.**, **Sacchi, L.**, **Gasparo Morticelli, M.**, **Buscemi, N.**, **Del Bono, P.**, **Lembo, C.P.**, **Pantaleone, A.**, **Pepe, F.**, **Scannavino, M.**, **Vaccaro, F.**, **Grimaldi, G.**, **Falcetti, S.**, **Grassi, S.** and **Tacchia, S.** (2005) Carta Geologica d'Italia, Foglio 604 (1:50.000): Isole Egadi, Servizio Geologico D'Italia.

Davies, G.R. (1970) Carbonate bank sedimentation, eastern Shark Bay, Western Australia. In: *Carbonate Sedimentation and Environments, Shark Bay, Western Australia* (Eds B.W. Logan, G.R. Davies, J.F. Read and D.E. Cebulski), *AAPG Mem.*, **13**, 85–168.

Davis, W.M. (1890) Structure and origin of glacial sand plains. *Geol. Soc. Am. Bull.*, **1**, 195–202.

Di Geronimo, I., **Di Geronimo, R.**, **La Perna, R.**, **Rosso, A.** and **Sanfilippo, R.** (2000) Cooling evidence from Pleistocene shelf assemblages in SE Sicily. In: *Climates: Past and Present* (Ed. M.B. Hart), *Geol. Soc. Spec. Publ.*, **181**, 113–120.

Dietrich, P., **Ghienne, J.F.**, **Normandeau, A.** and **Lajeunesse, P.** (2016) Upslope-migrating bedforms in a proglacial sandur delta: cyclic steps from river-derived underflows? *J. Sed. Res.*, **86**, 113–123.

Duller, R.A., **Mountney, N.P.**, **Russell, A.J.** and **Cassidy, N.C.** (2008) Architectural analysis of a volcaniclastic jökulhlaup deposit, southern Iceland: sedimentary evidence for supercritical flow. *Sedimentology*, **55**, 939–964.

Eberli, G.P., **Bernoulli, D.**, **Vecsei, A.**, **Sekti, R.**, **Grasmueck, M.**, **Lüdmann, T.**, **Anselmetti, F.S.**, **Mutti, M.** and **Della Porta, G.** (2019) A Cretaceous carbonate delta drift in the Montagna della Maiella, Italy. *Sedimentology*, **66**, 1266–1301.

Elias, E.P. and **van der Spek, A.J.** (2006) Long-term morphodynamic evolution of Texel Inlet and its ebb-tidal delta (The Netherlands). *Mar. Geol.*, **225**, 5–21.

Fagherazzi, S. and **Sun, T.** (2003) Numerical simulations of transportational cyclic steps. *Comput. Geosci.*, **29**, 1143–1154.

Fielding, C.R. (2006) Upper flow regime sheets, lenses and scour fills: extending the range of architectural elements for fluvial sediment bodies. *Sed. Geol.*, **190**, 227–240.

Fildani, A., **Normark, W.R.**, **Kostic, S.** and **Parker, G.** (2006) Channel formation by flow stripping: large-scale scour features along the Monterey East Channel and their relation to sediment waves. *Sedimentology*, **53**, 1265–1287.

Finetti, I., **Lentini, F.**, **Carbone, S.**, **Catalano, S.** and **Del Ben, A.** (1996) Il sistema Appennino meridionale-Arco Calabro-Sicilia nel Mediterraneo centrale: studio geologico geofisico. *Boll. Soc. Geol. Ital.*, **115**, 529–559.

Fornós, J.J. (1988) *Les Plataformes Carbonatades de les Balears. Estudi Sedimentològic de les Plataformes Miocenes de les Illes Balears i la Seva Comparació amb la Sedimentació Actual a la Seva Plataforma*. PhD Thesis, University of Barcelona, Spain, 953 pp.

Fornós, J.J. and **Ahr, W.M.** (1997) Temperate carbonates on a modern, low-energy, isolated ramp: the Balearic platform, Spain. *J. Sed. Res.*, **67**, 364–373.

Fralick, P. (1999) Paleohydraulics of chute-and-pool structures in a Paleoproterozoic fluvial sandstone. *Sed. Geol.*, **125**, 129–134.

Fricke, A.T., **Sheets, B.A.**, **Nittrouer, C.A.**, **Allison, M.A.** and **Ogston, A.S.** (2015) An examination of Froude-supercritical flows and cyclic steps on a subaqueous lacustrine delta, Lake Chelan, Washington, USA. *J. Sed. Res.*, **85**, 754–767.

Froude, M.J., **Alexander, J.**, **Barclay, J.** and **Cole, P.** (2017) Interpreting flash flood palaeoflow parameters from antidunes and gravel lenses: an example from Montserrat, West Indies. *Sedimentology*, **64**, 1817–1845.

Fuller, M.K., **Bone, Y.**, **Gostin, V.A.** and **Von Der Borch, C.C.** (1994) Holocene cool-water carbonate and terrigenous sediments from southern Spencer Gulf, South Australia. *Aust. J. Earth Sci.*, **41**, 353–363.

Gérard, J.R. and **Bromley, R.** (2008) *Ichnofabrics in Clastic Sediments: Applications to Sedimentological Core Studies*. J. Gerard, Madrid, 100 pp.

Gibbard, P. and **Cohen, K.M.** (2016) Global chronostratigraphical correlation table for the last 2.7 million years, v.2016a. Available at: https://dspace.library.uu.nl/handle/1874/179921

Gilbert, G.K. (1914) The transportation of débris by running water. *U.S. Geol. Surv. Prof. Pap.*, 86, 263 pp.

Guarnieri, P. (2006) Plio-Quaternary segmentation of the south Tyrrhenian forearc basin. *Int. J. Earth. Sci.*, **95**, 107–118.

Hand, B.M. (1974) Supercritical flow in density currents. *J. Sed. Petrol.*, **44**, 637–648.

Hanken, N.M., **Bromley, R.G.** and **Miller, J.** (1996) Plio-Pleistocene sedimentation in coastal grabens, north-east Rhodes, Greece. *Geol. J.*, **31**, 393–418.

Hansen, K.S. (1999) Development of a prograding carbonate wedge during sea level fall: lower Pleistocene of Rhodes, Greece. *Sedimentology*, **46**, 559–576.

Hernández-Molina, F.J., **Fernández-Salas, L.M.**, **Lobo, F.**, **Somoza, L.**, **Díaz-del-Río, V.** and **Dias, J.A.** (2000) The infralittoral prograding wedge: a new large-scale progradational sedimentary body in shallow marine environments. *Geo-Mar. Lett.*, **20**, 109–117.

Hiscott, R.N. (1994) Traction-carpet stratification in turbidites; fact or fiction? *J. Sed. Res.*, **64**, 204–208.

Imbrie, J. and **Buchanan, H.** (1965) Sedimentary structures in modern carbonate sands of the Bahamas. In: *Primary Sedimentary Structures and Their Hydrodynamic Interpretation* (Ed. G.V. Middleton), *SEPM Spec. Publ.*, **12**, 149–172.

Incandela, A. (1995) Lineamenti stratigrafico-struitturali dell'estremita Nordoccidentale della Sicilia e delle Isole di Favignana e Levanzo. PhD thesis, University of Palermo.

James, N.P. and **Bone, Y.** (1989) Petrogenesis of Cenozoic, temperate water calcarenites, South Australia: a model for meteoric/shallow burial diagenesis of shallow water calcite sediments. *J. Sed. Res.*, **59**, 191–203.

James, N.P. (1997) The cool-water carbonate depositional realm. In: *Cool-Water Carbonates* (Eds N.P. James and J. Clarke), *SEPM Spec. Publ.*, **56**, 1–20.

Johnston, S.T. and **Mazzoli, S.** (2009) The Calabrian Orocline: buckling of a previously more linear orogen. In: *Ancient Orogens and Modern Analogues* (Eds J.B. Murphy, J.D. Keppie and A.J. Hynes), *Geol. Soc. Spec. Publ.*, **327**, 113–125.

Jopling, A.V. and **Richardson, E.V.** (1966) Backset bedding developed in shooting flow in laboratory experiments. *J. Sed. Res.*, **36**, 821–825.

Kennedy, J.F. (1963) The mechanics of dunes and antidunes in erodible-bed channels. *J. Fluid Mech.*, **16**, 521–544.

Kil, R. and **Moscariello, A.** (2012) Reservoir Modelling of a Bioclastic Calcarenite Complex on Favignana, Southern Italy: The application of multi-point statistics. Search and Discovery Article #50548

Kostic, S. and **Parker, G.** (2006) The response of turbidity currents to a canyon-fan transition: internal hydraulic jumps and depositional signatures. *J. Hydraul. Res.*, **44**, 631–653.

Kostic, S. (2011) Modeling of submarine cyclic steps: controls on their formation, migration, and architecture. *Geosphere*, **7**, 294–304.

Lang, J. and **Winsemann, J.** (2013) Lateral and vertical facies relationships of bedforms deposited by aggrading supercritical flows: from cyclic steps to humpback dunes. *Sed. Geol.*, **296**, 36–54.

Lang, J., **Brandes, C.** and **Winsemann, J.** (2017) Erosion and deposition by supercritical density flows during channel avulsion and backfilling: field examples from coarse-grained deepwater channel-levée complexes (Sandino Forearc Basin, southern Central America). *Sed. Geol.*, **349**, 79–102.

Lees, A. and **Buller, A.T.** (1972) Modern temperate water and warm water shelf carbonate sediments contrasted. *Mar. Geol.*, **13**, 1767–1773.

Lennon, J.M. and **Hill, D.F.** (2006) Particle image velocimetry measurements of undular and hydraulic jumps. *J. Hydraul. Eng.*, **132**, 1283–1294.

Long, D., **Steffler, P.M.**, **Rajaratnam, N.** and **Smy, P.** (1991) Structure of flow in hydraulic jumps. *J. Hydraul. Res.*, **29**, 293–308.

Longhitano, S.G. (2011) The record of tidal cycles in mixed silici–bioclastic deposits: examples from small Plio-Pleistocene peripheral basins of the microtidal Central Mediterranean Sea. *Sedimentology*, **58**, 691–719.

Longhitano, S.G. (2013) A facies-based depositional model for ancient and modern, tectonically-confined tidal straits. *Terra Nova*, **25**, 446–452.

Longhitano, S.G. and **Steel, R.J.** (2016) Deflection of the progradational axis and asymmetry in tidal seaway and strait deltas: insights from two outcrop case studies. *Geol. Soc. Spec. Publ.*, **444**, 141–172.

Lüdmann, T., **Betzler, C.**, **Eberli, G.P.**, **Reolid, J.**, **Reijmer, J.J.G.**, **Sloss, C.G.**, **Bialik, O.M.**, **Alvarez-Zarikian, C.A.**, **Alonso-García, M.**, **Blättler, C.L.**, **Guo, J.A.**, **Haffen, S.**, **Horozal, S.**, **Inoue, M.**, **Jovane, L.**, **Kroon, D.**, **Lanci, L.**, **Laya, J.C.**, **Mee, A.L.H.**, **Nakakuni, M.**, **Nath, B.N.**, **Niino, K.**, **Petruny, L.P.**, **Pratiwi, S.D.**, **Slagle, A.L.**, **Su, X.**, **Swart, P.K.**, **Wright, J.D.**, **Yao, Z.** and **Young, J.R.** (2018) Carbonate delta drift: a new sediment drift type. *Mar. Geol.*, **401**, 98–111.

Lykousis, V. (1991) Sea level changes and sedimentary evolution during the Quaternary in the northwest Aegean continental margin, Greece. In: *Sedimentation and Eustatic Sea Level Changes at Active Plate Margins* (Ed. D.I.M. MacDonald), *Spec. Publ. Int. Ass. Sediment.*, **12**, 123–131.

MacDonald, R.G., **Alexander, J.**, **Bacon, J.C.** and **Cooker, M.J.** (2009) Flow patterns, sedimentation and deposit architecture under a hydraulic jump on a non-eroding bed: defining hydraulic-jump unit bars. *Sedimentology*, **56**, 1346–1367.

Martín, J.M., **Braga, J.C.**, **Betzler, C.** and **Brachert, T.** (1996) Sedimentary model and high-frequency cyclicity in a Mediterranean, shallow-shelf, temperate-carbonate environment (uppermost Miocene, Agua Amarga Basin, southern Spain). *Sedimentology*, **43**, 263–277.

Martín, J.M., **Braga, J.C.**, **Aguirre, J.** and **Betzler, C.** (2004) Contrasting models of temperate carbonate sedimentation in a small Mediterranean embayment: the Pliocene Carboneras Basin, SE Spain. *J. Geol. Soc. London*, **161**, 387–399.

Massari, F. (1996) Upper-flow-regime stratification types on steep-face, coarse-grained, Gilbert-type progradational wedges (Pleistocene, southern Italy). *J. Sed. Res.*, **66**, 364–375.

Massari, F. and **Chiocci, F.** (2006) Biocalcarenite and mixed cool-water prograding bodies of the Mediterranean Pliocene and Pleistocene: architecture, depositional setting and forcing factors. In: *Cool-water Carbonates: Depositional Systems and Palaeoenvironmental Controls* (Eds H.M. Pedley and G. Carannante), *Geol. Soc. Spec. Publ.*, **255**, 95–120.

Massari, F. and **D'Alessandro, A.** (2012) Facies partitioning and sequence stratigraphy of a mixed siliciclastic-carbonate ramp stack in the Gelasian of Sicily (S Italy): a potential model for icehouse, distally-steepened heterozoan ramps. *Riv. Ital. Paleontol. Stratigr.*, **118**, 503–534.

Massari, F., **Sgavetti, M.**, **Rio, D.**, **D'Alessandro, A.** and **Prosser, G.** (1999) Composite sedimentary record of falling stages of Pleistocene glacio-eustatic cycles in a shelf setting (Crotone basin, south Italy). *Sed. Geol.*, **127**, 85–110.

Mauz, B. (1998) The onset of the quaternary: a review of new findings in the Pliocene-Pleistocene chronology. *Quatern. Sci. Rev.*, **17**, 357–364.

Meloni, D., **Sabato, L.**, **Tropeano, M.**, **Brandano, M.** and **Mateu-Vicens, G.** (2013) A 2D view of mixed (bioclastic/lithoclastic) carbonate clinoforms in the Matera area (Plio-Pleistocene, southern Italy). *J. Mediterr. Earth Sci. Spec. Issue*, **121**, 121–122.

Michaud, K. and **Dalrymple, R.W.** (2016) Facies, architecture and stratigraphic occurrence of headland-attached tidal sand ridges in the Roda Formation, Northern Spain. In: *Contributions to Modern and Ancient Tidal Sedimentology* (Eds B. Tessier and J.Y. Reynaud), *Spec. Publ. Int. Ass. Sediment.*, **47**, 313–342.

Mullins, H.T. and **Cook, H.E.** (1986) Carbonate apron models: alternatives to the submarine fan model for paleoenvironmental analysis and hydrocarbon exploration. *Sed. Geol.*, **48**, 37–79.

Nemec, W. (1990) Aspects of sediment movement on steep delta slopes. In: *Coarse-grained Deltas* (Eds A. Colella and D.B. Prior). *Int. Assoc. Sedimentol. Spec. Publ.*, **10**, 29–73.

Normandeau, A., **Lajeunesse, P.**, **Poiré, A.G.** and **Francus, P.** (2016) Morphological expression of bedforms formed by supercritical sediment density flows in four fjord-lake deltas of the south-eastern Canadian Shield (Eastern Canada). *Sedimentology*, **63**, 2106–2129.

O'Connell, L.G., **James, N.P.**, **Doubell, M.**, **Middleton, J.F.**, **Luick, J.**, **Currie, D.R.** and **Bone, Y.** (2016) Oceanographic controls on shallow-water temperate carbonate sedimentation: Spencer Gulf, South Australia. *Sedimentology*, **63**, 105–135.

Parker, G. (1996) Some speculations on the relation between channel morphology and channel-scale flow structures. In: *Coherent Flow Structures in Open Channels*(Eds. P. Ashworth, S.J. Bennett, J.L. Best and S.J. McLelland), pp. 429–432. John Wiley & Sons, New York, NY.

Pedley, H.M., **Grasso, M.**, **Maniscalco, R.**, **Behncke, B.**, **DiStefano, A.**, **Giuffrida, S.** and **Sturiale, G.** (2001) The sedimentology and palaeoenvironment of Quaternary temperate carbonates and their distribution around the northern Hyblean Mountains (SE Sicily). *Boll. Soc. Geol. Ital.*, **121**, 233–255.

Pedley, M. and **Grasso, M.** (2002) Lithofacies modelling and sequence stratigraphy in microtidal cool-water carbonates: a case study from the Pleistocene of Sicily, Italy. *Sedimentology*, **49**, 533–553.

Pedley, H.M. and **Carannante, G.** (2006) Cool-water carbonate ramps: a review. In: *Cool-Water Carbonates: Depositional Systems and Palaeoenvironmental Controls* (Eds H.M. Pedley and G. Carannante), *Geol. Soc. Spec. Publ.*, **255**, 1–9.

Pedley, M. and **Grasso, M.** (2006) The response of cool-water carbonates to eustatic change in microtidal, Mediterranean Quaternary settings of Sicily. In: *Cool-Water Carbonates: Depositional Systems and Palaeoenvironmental Controls* (Eds H.M. Pedley and G. Carannante), *Geol. Soc. Spec. Publ.*, **255**, 137–156.

Pepe, F., **Bertotti, G.**, **Cella, F.** and **Marsella, E.** (2000) Rifted margin formation in the south Tyrrhenian Sea: a high resolution seismic profile across the north Sicily passive continental margin. *Tectonics*, **19**, 241–257.

Pomar, L. (2001) Types of carbonate platforms: a genetic approach. *Basin Res.*, **13**, 313–334.

Pomar, L. and **Tropeano, M.** (2001) The Calcarenite di Gravina Formation in Matera (southern Italy): new insights for coarse-grained, large-scale, cross-bedded bodies encased in offshore deposits. *AAPG Bull.*, **85**, 661–690.

Pomar, L., **Obrador, A.** and **Westphal, H.** (2002) Sub-wavebase cross-bedded grainstones on a distally steepened carbonate ramp, Upper Miocene, Menorca, Spain. *Sedimentology*, **49**, 139–169.

Pomar, L., **Bassant, P.**, **Brandano, M.**, **Ruchonnet, C.** and **Janson, X.** (2012) Impact of carbonate producing biota on platform architecture: insights from Miocene examples of the Mediterranean region. *Earth-Sci. Rev.*, **113**, 186–211.

Poole, A.J. and **Robertson, A.H.F.** (1991) Quaternary uplift and sea-level change at an active plate boundary, Cyprus. *J. Geol. Soc. London*, **148**, 909–921.

Postma, G., **Roep, T.B.** and **Ruegg, G.H.** (1983) Sandy-gravelly mass-flow deposits in an ice-marginal lake (Saalian, Leuvenumsche Beek Valley, Veluwe, The Netherlands), with emphasis on plug-flow deposits. *Sed. Geol.*, **34**, 59–82.

Postma, G., **Cartigny, M.J.B.** and **Kleverlaan, K.** (2009) Structureless, coarse-tail graded Bouma Ta formed by internal hydraulic jump of the turbidity current? *Sed. Geol.*, **219**, 1–6.

Postma, G. and **Cartigny, M.J.** (2014) Supercritical and subcritical turbidity currents and their deposits—A synthesis. *Geology*, **42**, 987–990.

Postma, G., **Kleverlaan, K.** and **Cartigny, M.J.B.** (2014) Recognition of cyclic steps in sandy and gravelly turbidite sequences, and consequences for the Bouma facies model. *Sedimentology*, **61**, 2268–2290.

Puga-Bernabéu, Á., **Martin, J.M.** and **Braga, J.C.** (2008) Sedimentary processes in a submarine canyon excavated into a temperate-carbonate ramp (Granada Basin, southern Spain). *Sedimentology*, **55**, 1449–1466.

Puga-Bernabéu, Á., **Martín, J.M.**, **Braga, J.C.** and **Sánchez-Almazo, I.M.** (2010) Downslope-migrating sandwaves and platform-margin clinoforms in a current-dominated, distally steepened temperate-carbonate ramp (Guadix Basin, Southern Spain). *Sedimentology*, **57**, 293–311.

Raffi, S. (1986) The significance of marine boreal molluscs in the early Pleistocene faunas of the Mediterranean area. *Palaeogeogr. Palaeoclimatol. Palaeoecol.*, **52**, 267–289.

Read, J.F. (1985) Carbonate platform facies models. *AAPG Bull.*, **69**, 1–21.

Reich, S., **Di Martino, E.**, **Todd, J.A.**, **Wesselingh, F.P.** and **Renema, W.** (2015) Indirect paleo-seagrass indicators (IPSIs): a review. *Earth-Sci. Rev.*, **143**, 161–186.

Reynaud, J.Y., **Ferrandini, M.**, **Ferrandini, J.**, **Santiago, M.**, **Thinon, I.**, **André, J.P.**, **Barthet, Y.**, **Guennoc, P.** and **Tessier, B.** (2013) From non-tidal shelf to tide-dominated strait: the Miocene Bonifacio Basin, Southern Corsica. *Sedimentology*, **60**, 599–623.

Rossi, V.M., **Longhitano, S.G.**, **Mellere, D.**, **Dalrymple, R.W.**, **Steel, R.J.**, **Chiarella, D.** and **Olariu, C.** (2017) Interplay of tidal and fluvial processes in an early Pleistocene, delta-fed, strait margin (Calabria, Southern Italy). *Mar. Petrol. Geol.*, **87**, 14–30.

Russell, H.A.J. and **Arnott, R.W.C.** (2003) Hydraulic jump and hyperconcentrated flow deposits of a glacigenic subaqueous fan: Oak Ridges Moraine, southern Ontario, Canada. *J. Sed. Res.*, **73**, 887–905.

Saunderson, H.C. and **Lockett, F.P.** (1983) Flume experiments on bedforms and structures at the dune-plane bed transition. In: *Modern and Ancient Fluvial Systems* (Eds J.D. Collinson and J. Lewin), *Spec. Publ. Int. Ass. Sediment.*, **6**, 49–58.

Schlager, W. (2000) Sedimentation rates and growth potential of tropical, cool-water and mud-mound carbonate factories. In: *Carbonate Platform Systems: Components and Interactions* (Eds E. Insalaco, P.W.

Skelton and T.J. Palmer), *Geol. Soc. Spec. Publ.*, **178**, 217–227.

Schlager, W. (2005) Carbonate sedimentology and sequence stratigraphy. *SEPM Concepts in Sed. and Pal.*, 8, 200 pp.

Schumm, S.A., **Bean, D.W.** and **Harvey, M.D.** (1982) Bed-form-dependent pulsating flow in Medano Creek, Southern Colorado. *Earth Surf. Proc. Land.*, **7**, 17–28.

Sequeiros, O.E. (2012) Estimating turbidity current conditions from channel morphology: a Froude number approach. *J. Geophys. Res.-Oceans*, **117**, C04003.

Sha, L.P. and **de Boer, P.L.** (1991) Ebb-tidal delta deposits along the west Frisian Islands (The Netherlands): processes, facies architecture and preservation. In: *Clastic Tidal Sedimentology* (Ed. D.G. Smith), *Canadian Society of Petroleum Geologists, Memoir*, **16**, 199–218.

Simons, D.B., **Richardson, E.V.** and **Nordin, C.F.** (1965) Sedimentary structures generated by flow in alluvial channels. In: *Primary Sedimentary Structures and Their Hydrodynamic Interpretation* (Ed. G.V. Middleton), *SEPM Spec. Publ.*, **12**, 34–52.

Ślączka, A., **Nigro, F.**, **Renda, P.** and **Favara, R.** (2011) Lower Pleistocene deposits in east part of the Favignana Island, Sicily, Italy. *Ital. J. Quatern. Sci.*, **24**, 153–169.

Slootman, A. (2016) Supercritical density flow on cool-water carbonate ramps – The Lower Pleistocene of Favignana Island, Italy. PhD Thesis University of Geneva, no. Sc. 5055. Available at: http://archive-ouverte.unige.ch/unige: 92759.

Slootman, A., **Cartigny, M.J.B.**, **Moscariello, A.**, **Chiaradia, M.** and **de Boer, P.L.** (2016a) Quantification of tsunami-induced flows on a Mediterranean carbonate ramp reveals catastrophic evolution. *Earth Planet. Sci. Lett.*, **444**, 192–204.

Slootman, A., **Cartigny, M.J.B.**, **de Boer, P.L.** and **Moscariello, A.** (2016b) Depositional character of submarine dunes on a Pleistocene distally steepened carbonate ramp (Favignana Island, Italy). In: *Marine and River Dune Dynamics* (Eds K.J.J. Van Landeghem, T. Garlan and J.H. Baas), MARID 2016, Fifth International Conference on Marine and River Dune Dynamics, Caernarfon, United Kingdom, 4− 6 April 2016. Bangor University and SHOM. 216 pp. ISBN 978-2-11-128417-3.

Sohn, Y.K. (1997) On traction carpet sedimentation. *J. Sed. Res.*, **67**, 502–509.

Spinewine, B., **Sequeiros, O.E.**, **Garcia, M.H.**, **Beaubouef, R.T.**, **Sun, T.** and **Savoye, B.** (2009) Experiments on wedge-shaped deep sea sedimentary deposits in minibasins and/or on channel levees emplaced by turbidity currents. Part II. Morphodynamic evolution of the wedge and of the associated bedforms. *J. Sed. Res.*, **79**, 608.

Stokes, W.L. (1947) Primary lineation in fluvial sandstones a criterion of current direction. *J. Geol.*, **55**, 52–54.

Sun, T. and **Parker, G.** (2005) Transportational cyclic steps created by flow over an erodible bed. Part 2. Theory and numerical simulation. *J. Hydraul. Res.*, **43**, 502–514.

Taki, K. and **Parker, G.** (2005) Transportational cyclic steps created by flow over an erodible bed. Part 1. Experiments. *J. Hydraul. Res.*, **43**, 488–501.

Tavarnelli, E., **Renda, P.**, **Pasqui, V.** and **Tramutoli, M.** (2003) The effects of post-orogenic extension on different scales: an example from the Apennine-Maghrebide fold-and-thrust belt, SW Sicily. *Terra Nova*, **15**, 1–7.

Turmel, D., **Locat, J.** and **Parker, G.** (2012) Upstream migration of knickpoints: geotechnical considerations. In: *Submarine Mass Movements and their Consequences in Natural and Technological Hazards Research*(Eds. Y. Yamada, K. Kawamura, K. Ikehara, Y. Ogawa, R. Urgeles, D. Mosher, J. Chaytor and M. Strasser), pp. 123–132. Springer, The Netherlands.

Turmel, D., **Locat, J.** and **Parker, G.** (2015) Morphological evolution of a well-constrained, subaerial–subaqueous source to sink system: Wabush Lake. *Sedimentology*, **62**, 1636–1664.

Vellinga, A.J., **Cartigny, M.J.B.**, **Eggenhuisen, J.T.** and **Hansen, E.W.M.** (2018) Morphodynamics and depositional signature of fluvial cyclic steps: New insight from a depth-resolved numerical model. *Sedimentology*, **65**, 540–560.

Winterwerp, J.C., **Bakker, W.T.**, **Mastbergen, D.R.** and **Van Rossum, H.** (1992) Hyperconcentrated sand-water mixture flows over erodible bed. *J. Hydraul. Eng.*, **118**, 1508–1525.

Wornardt, W.W. and **Vail, P.R.** (1991) Revision of the Plio-Pleistocene cycles and their application to sequence stratigraphy and shelf and slope sediments in the Gulf of Mexico. *Trans. Gulf Coast Assoc. Geol. Soc.*, **41**, 719–744.

Yokokawa, M., **Takahashi, Y.**, **Yamamura, H.**, **Kishima, Y.**, **Parker, G.** and **Izumi, N.** (2011) Phase diagram for antidunes and cyclic steps based on suspension index, non-dimensional Chezy resistance coefficient and Froude number. In: *International Association for Hydro-Environment Engineering and Research*, 7th Symposium on River, Coastal and Estuarine Morphodynamics, Beijing, China (RCEM 2011), Proceedings, 1789-1794.

Yokokawa, M., **Izumi, N.**, **Naito, K.**, **Parker, G.**, **Yamada, T.** and **Greve, R.** (2016) Cyclic steps on ice. *J. Geophys. Res.-Earth*, **121**, 1023–1048.

Zhong, G., **Cartigny, M.J.**, **Kuang, Z.** and **Wang, L.** (2015) Cyclic steps along the South Taiwan Shoal and West Penghu submarine canyons on the northeastern continental slope of the South China Sea. *Geol. Soc. Am. Bull.*, **127**, 804–824.

Manuscript received 18 May 2017; revision accepted 29 January 2019

Supporting Information

Additional information may be found in the online version of this article:

Table S1. Results of point counting of selected units in the Lower Pleistocene carbonate wedge of Favignana Island.